Electronic Supplementary Information

Copper and manganese diazacalix[4]arene complexes: structural and cytotoxicity studies and use in ring opening polymerization of *ε*-caprolactone and *δ*-valerolactone

Azaria C. Razieh,[a] Harry C. Sample,[a] Emily Hobson,[b] Anja Mueller,[b] Timothy J. Prior[c] and Carl Redshaw[b,d*]

[a] *Department of Chemistry, University of Hull, Cottingham Rd., Hull, HU6 7RX, UK*

[b] *School of Chemistry, Pharmacy and Pharmacology, University of East Anglia, Norwich, NR4 7TJ, UK*

[c] *Department of Chemistry, University of Liverpool, Crown Street, Liverpool, L69 7ZD, UK*

[d] *Department of Chemistry, Graduate School of Science, Tokyo Metropolitan University, 1-1 Minami Osawa, Hachioji, Tokyo, 192-0397, Japan*

Contents

Experimental

The parent ligand *p*-$MeLH_4$ was synthesized according to published procedures.[S1] Our characterization of the *p*-$MeLH_4$ is presented in Figs. **S18-S24**. The complexes **1**·DMF, **2**, and **3**·3.5DMF were synthesized following a modification to an existing procedure.[S2] To *p*-$MeLH_4$ (0.085 g, 0.149 mmol) was added a metal salt (2 eq.), DMF or DMSO (10 mL), MeOH (10 mL) and organic base (0.2 mL). The solutions were stirred for 1 h at room temperature (*ca*. 15 °C) and filtered through a cotton pad. The solutions were left to stand at room temperature, and crystals suitable for single crystal X-ray diffraction were obtained upon standing. For further analyses, these crystals were isolated *via* filtration and washed with hexane (3 × 10 mL) before being dried *in vacuo* (10–15 mbar, 50 °C, 16 h).

Synthesis of [Cu(*p*-$MeLH_3$)(Py)(NO_3)]•DMF (**1**·DMF)

Synthesized using $Cu(NO_3)_2·3H_2O$ (0.072 g, 0.298 mmol), C_5H_5N (0.2 mL, 2.47 mmol, 16.6 eq.) and DMF (10 mL) yielding **1**·DMF as dark blocks (20 mg, 23.7 μmol, 16 %). Anal. Calcd. C 69.62, H 6.41, N 5.94%; found C 69.51, H 6.77, N 5.68%. Mass Spec (MALDI-TOF) Calc for $C_{36}H_{41}CuN_2O_4$ = 628.236, found 628.285 $[M-Py]^+$; IR (FT-ATR-IR): 3394, 3130, 2859, 1609, 1544, 1468, 1375, 1300, 1265, 1234, 1162, 1147, 1111, 1037, 1021, 953, 917, 863, 852, 823, 808, 793, 765, 746, 715, 701, 659, 629 cm^{-1}; Crystal Data for **1**·DMF: $C_{44}H_{53}CuN_5O_8$ (M = 843.45 g mol^{-1}): orthorhombic, space group $P2_12_12_1$ (No. 19), *a* = 29.4614(15) Å, *b* = 14.7279(8) Å, *c* = 9.4738(4) Å, α = β = γ = 90°, V = 4110.7(4) $Å^3$, Z = 4, T = 100.0(6) K, μ(Mo Kα)= 0.591 mm^{-1}, D_{calc} = 1.363 g cm^{-3}, 42617 reflections measured (3.092° ≤ 2θ ≤ 54.97°), 9441 unique (R_{int} = 0.0890, R_{sigma} = 0.0750) which were used in all calculations. The final R_1 was 0.1409 (I > 2σ(I)) and wR_2 was 0.3662 (all data).

Synthesis of $[Cu(L^OH_3)]_2$ (**2**)

Synthesized using $Cu(OAc)_2•H_2O$ (0.060 g, 0.300 mmol), C_5H_5N (0.2 mL, 2.47 mmol, 16.6 eq.) and DMSO (10 mL) yielding **2** as green prisms (30 mg,45.3 μmol 31 %). Anal. Calcd. C 67.11, H 6.26, N 4.35%; found C 67.24, H 6.13, N 4.47%. Mass Spec (MALDI-TOF) Calcd. for $C_{36}H_{44}CuN_2O_6$ = 664.2904, obs. 664.746 $[M+2H]^+$;. IR (FT-ATR-IR): 3283, 2995, 2969, 2918, 2547, 1739, 1667, 1602, 1473, 1396, 1377, 1296, 1317, 1256, 1278, 1233, 1217, 1157, 1140, 1104, 1071, 1043, 975, 941, 924, 910, 874, 861, 846, 825, 801, 786, 755, 693, 652, 643, 625 cm^{-1}; Crystal Data for **2**:

$C_{36}H_{42}CuN_2O_6$ (M = 662.65 g mol^{-1}): monoclinic, space group *C*2/*c* (No. 15), *a* = 22.2979(6) Å, *b* = 21.0630(6) Å, *c* = 13.7829(4) Å, α = γ = 90°, β = 91.267(2)°, V = 6471.7(3) Å^3, Z = 8, T = 100.01(10) K, μ(Mo Kα)= 0.724 mm^{-1}, D_{calc} = 1.359 g cm^{-3}, 61949 reflections measured (3.654° ≤ 2θ ≤ 59.148°), 9078 unique (R_{int} = 0.0411, R_{sigma} = 0.0283) which were used in all calculations. The final R_1 was 0.0569 (I > 2σ(I)) and wR_2 was 0.1497 (all data).

Synthesis of [Mn(*p*-MeLH$_3$)(*p*-MeLH$_2$)]·3.5DMF (**3**·3.5DMF)

Synthesized using Mn(OAc)$_2$·4H$_2$O (0.073 g, 0.298 mmol), Et$_3$N (0.2 mL, 1.43 mmol, 9.6 eq.) and DMF (10 mL), yielding the complex **3**·3.5DMF as black prisms (58 mg, 40.2 μmol, 27 %). Anal. Calcd. C 73.02, H 6.81, N 4.73%; found C 73.15, H 7.12, N 4.44%. Mass Spec (MALDI-TOF) Calcd for. $C_{37}H_{49}MnN_2O_7$ = 688.292, found 688.632 [M-L-3.5DMF+MeOH+2H$_2$O]$^+$; IR (FT-ATR-IR): 2989, 2915, 2842, 1666, 1604, 1456, 1384, 1291, 1248, 1154, 1132, 1086, 1029, 970, 921, 864, 845, 830, 783, 739, 710, 659, 621 cm^{-1}; μ_{eff} = 4.82 μ_B. Crystal Data for **3**·3.5DMF: $C_{82.5}H_{105.5}MnN_{7.5}O_{11.5}$ (M = 1441.18 g mol^{-1}): triclinic, space group *P*-1 (No. 2), *a* = 14.7872(11) Å, *b* = 17.1285(11) Å, *c* = 17.3346(11) Å, α = 109.068(6)°, β = 103.726(6)° γ = 106.287(6)°, V = 3712.1(5) Å^3, Z = 2, T = 100.00(10) K, μ(Cu Kα)= 1.987 mm^{-1}, D_{calc} = 1.289 g cm^{-3}, 34903 reflections measured (5.788° ≤ 2θ ≤ 100.872°), 7731 unique (R_{int} = 0.2003, R_{sigma} = 0.1764) which were used in all calculations. The final R_1 was 0.0764 (I > 2σ(I)) and wR_2 was 0.2076(all data).

Crystallographic details

For each of the four structures, **1**, **1b**, **2**, **3** data were collected by the UK National Crystallography Service, Southampton, UK. Each data collection employed a custom Rigaku Oxford Diffraction X-ray diffractometer. In the case of **1** and **2** data were collected using a Mo rotating anode source and a HyPix 6000 detector. For **1b** and **3**, the source was a Cu rotating anode and an Arc-100 detector was employed. Crystals were held at 100K using an Oxford Cryosystems nitrogen gas cryostream. Data were processed using standard techniques using CrysAlisPro.[S3] Structures were solved using dual-space methods (SHELXT)[S4] and refined using SHELXL[S5] implemented within Olex2.[S6]

Procedure for ROP of ε-caprolactone and δ-valerolactone

For the ROP procedures, the monomers ε-CL and δ-VL were used as received.

The pre-catalyst (0.01 mmol) was weighed out under air and was combined with the monomer (5 mmol) in a round bottom flask. A condenser was attached and the system was heated at 150 ^{o}C for 24h. The polymerization mixture was quenched on addition of an excess of glacial acetic acid (0.2 mL) into the solution, and the resultant solution was then poured into cold methanol (20 mL). The resultant polymer was then collected after solvent vaporization in a fume hood and was dried in vacuum oven.

For entries 3 and 8 in Table 1, 3 mL of toluene and then the appropriate equivalent of BnOH (from a pre-prepared stock solution of 1 mmol BnOH in 100 mL toluene) and 5 mmol of monomer was added to the flask. The reaction mixture was then placed into an oil/sand bath pre-heated at 110 °C, and the solution was stirred for 24 h. Work-up was as above.

Kinetics procedure

The polymerizations were carried out at 150 ℃ as melts using 0.02 mmol of complex and 10 mmol of monomer under air. At appropriate time intervals, 0.5 μL aliquots were removed and were quenched with wet $CDCl_3$. The percent conversion of monomer to polymer was determined using ^{1}H NMR spectroscopy.

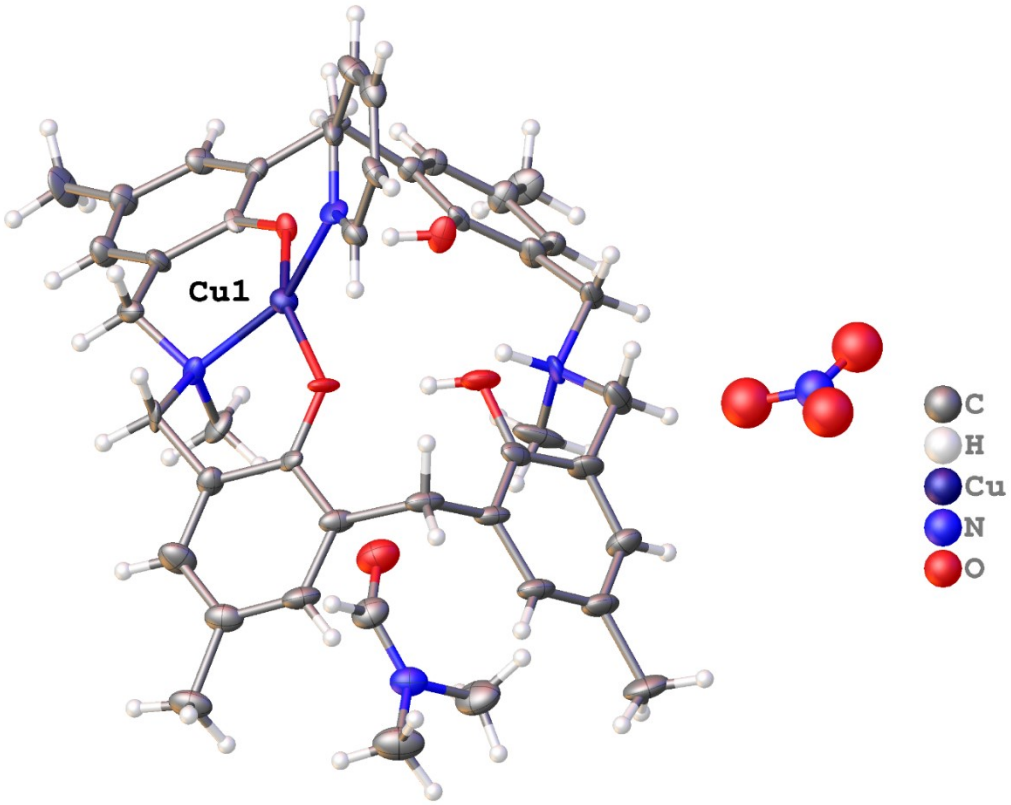

Figure S1. Asymmetric unit of **1** with atoms drawn as 50% ellipsoids. For clarity only one orientation of the nitrate anion is shown. The data quality means there are several regions of large electron density that are not part of the structure. There is some evidence that the Cu1 was disordered so that it was bound by atoms O2, O3, and N2 a small portion of the time, but it was not possible to derive a stable disorder model. This electron density may be a result of the twinning rather than true disorder.

There is also a molecule of DMF within the cavity of the azacalixarene ligand, a common feature of this class of structure.[S7]

When remaking **1**, a second batch of crystals yielded crystals suitable for X-ray diffraction, but these were poor quality and subject to twinning. The structure of this polymorph **1b** was clearly established, but it was not possible to use anisotropic displacement parameters to model the structure.

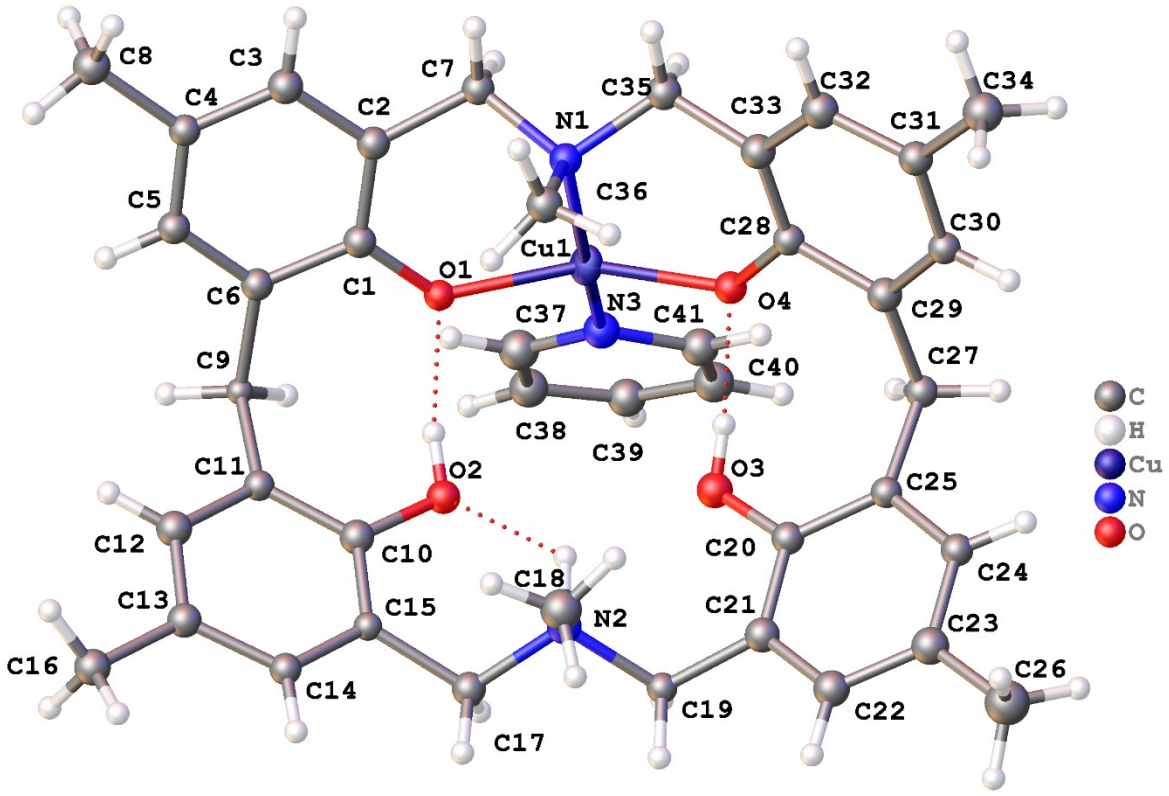

Figure S2. Structure of the polymorph **1b**.

Intriguingly the second polymorph is *monoclinic* with lattice parameters very similar to those of the first, orthorhombic, polymorph. The first structure can be reset (*b*, *c*, *a*, β ≈ 90 °) to show the similarity with the first cell. The reason for the difference in symmetry is not clear. The space groups are related to *Pnma*: $P2_1/c$ and $P2_12_12_1$ are maximal non-isomorphous subgroups of *Pnma*, and *Pc* is a direct subgroup of $P2_1/c$. Inspection of the monoclinic structure but overlaying the two unique metal complexes suggests there are only small difference in the conformation of the molecules present. (Figure S3) It is worth noting that both structures were collected at 100 K.

In the same way as for the structure of **1**, there was some evidence that there may be a small amount of copper bound at the second site (N2).

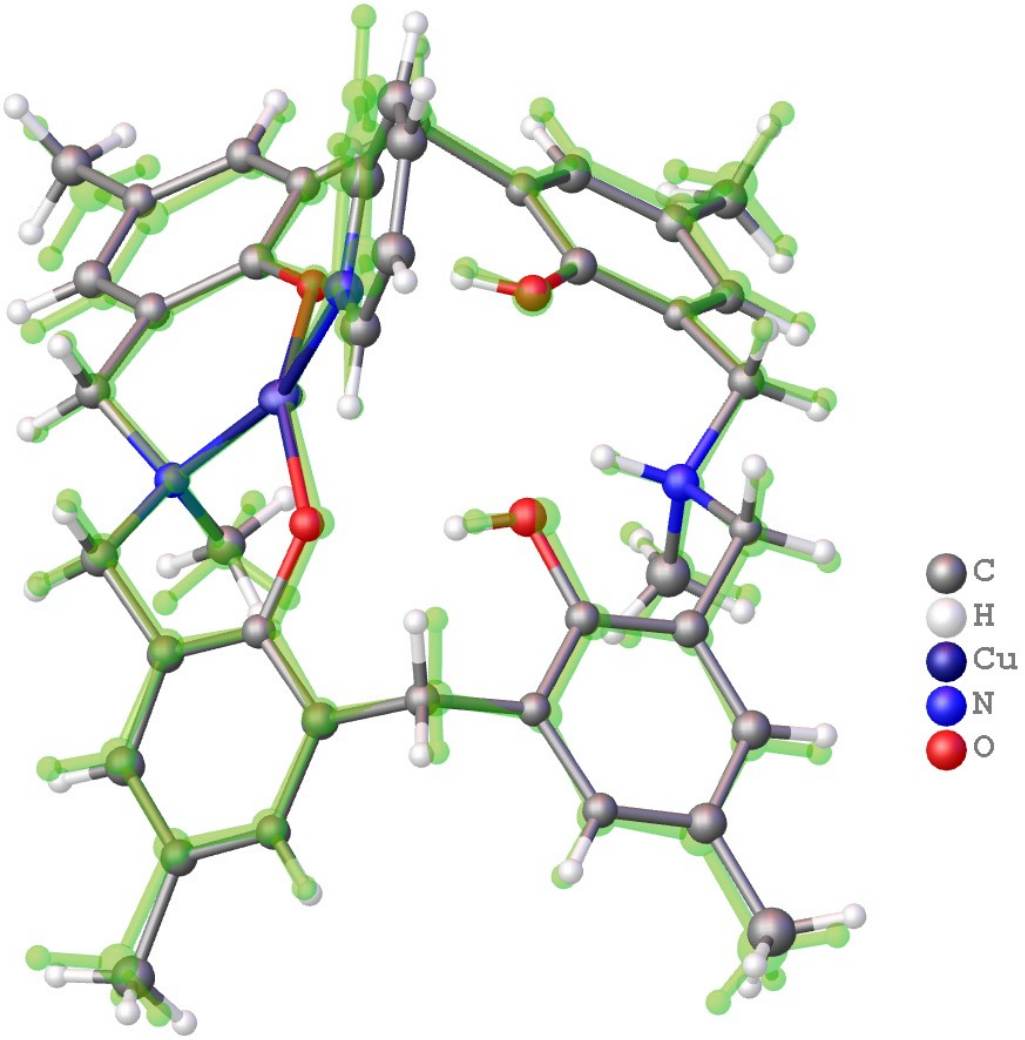

Figure S3: Overlay of the two unique copper complexes in the structures **1** and **1b**. One complex is shown with representative atomic colours and the other is coloured green.

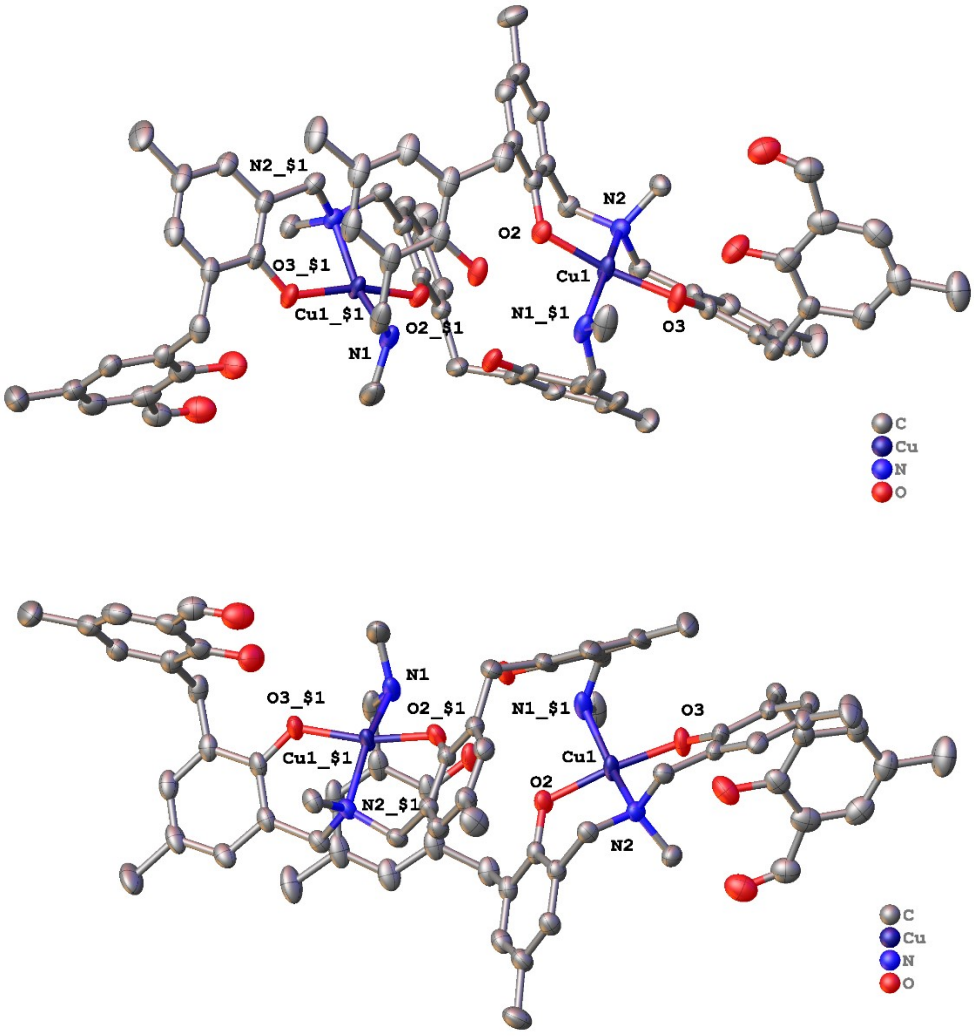

Figure S4. Alternative views of **2**.

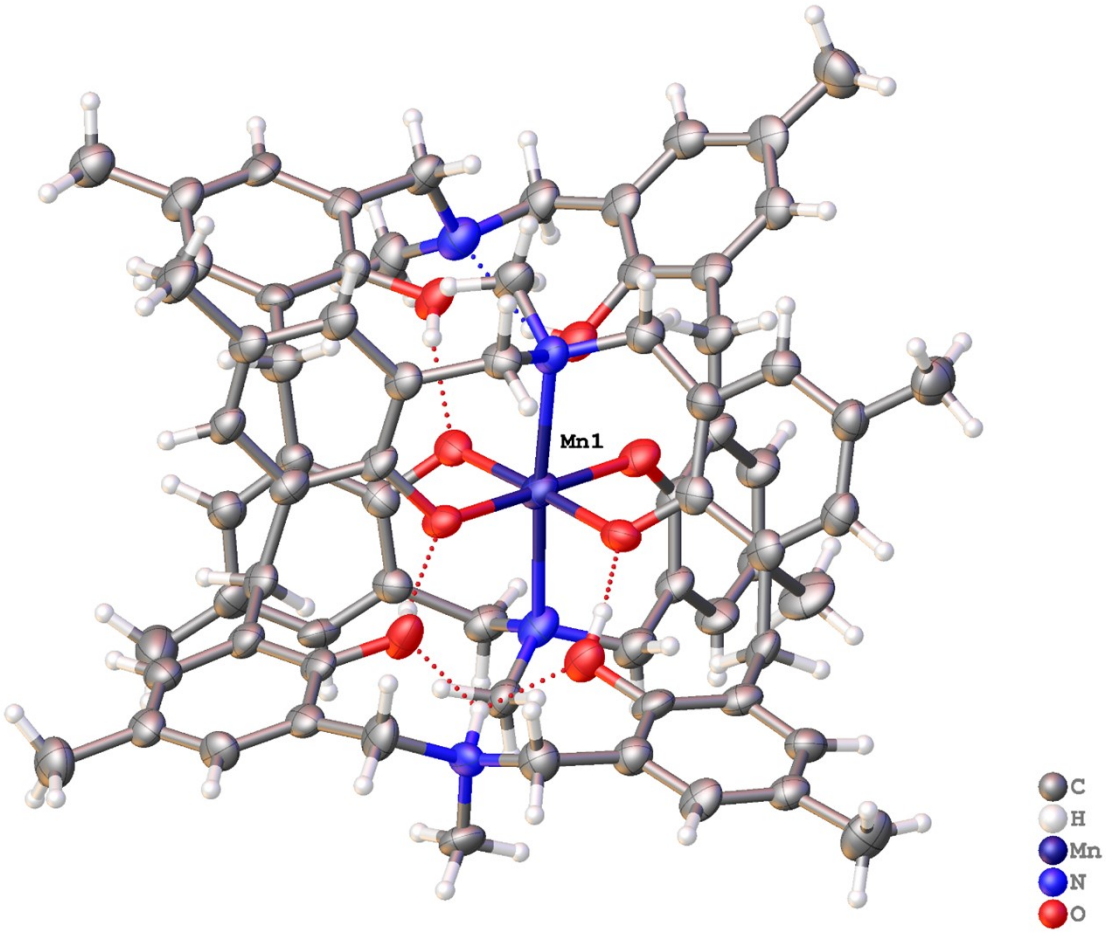

Figure S5. Alternative views of **3**. Dashed lines show hydrogen bonds.

In **3**, a single well-ordered DMF was located; other disordered solvent was modelled using a solvent mask (SQUEEZE).

Compound	M-L bond lengths / Å	L-M-L bond angles (°) and geometry description*
1	Cu1−O4 1.887(9) Cu1−O1 1.893(9) Cu1−N1 2.015(12) Cu1−N3 2.053(12)	Flattened tetrahedron; τ_4 = 0.33 O4−Cu1−O1 156.1(4) O4−Cu1−N1 93.4(4) O4−Cu1−N3 90.3(5) O1−Cu1−N1 94.5(4) O1−Cu1−N3 91.2(4) N1−Cu1−N3 156.7(5)
1b	Cu1−O1 1.906(10) Cu1−O4 1.891(10) Cu1−N1 2.032(14) Cu1−N3 2.040(15)	Flattened tetrahedron; τ_4 = 0.28 O1−Cu1−N1 90.7(5) O1−Cu1−N3 90.3(5) O4−Cu1−O1 157.7(5) O4−Cu1−N1 95.2(5) O4−Cu1−N3 90.5(5) N1−Cu1−N3 162.2(6)
2	Cu1−O2 1.9063(16) Cu1−O3 1.9125(17) Cu1−N11 2.021(2) Cu1−N2 2.0166(18)	Flattened tetrahedron; τ_4 = 0.25 O2−Cu1−O3 165.17(8) O2−Cu1−N11 89.24(8) O2−Cu1−N2 95.22(7) O3−Cu1−N11 88.67(8) O3−Cu1−N2 91.80(8) N2−Cu1−N11 159.71(9)
3	Mn1−O1 1.997(5) Mn1−O4 1.937(4) Mn1−O5 1.973(5) Mn1−O8 1.880(4) Mn1−N2 2.296(6) Mn1−N4 2.321(6) Rms deviation of bond lengths from perfect octahedron = 0.084 Å	An elongated, distorted octahedron. O1−Mn1−N2 85.5(2) O1−Mn1−N4 92.4(2) O4−Mn1−O1 86.0(2) O4−Mn1−O5 90.7(2) O4−Mn1−N2 89.36(19) O4−Mn1−N4 94.0(2) O5−Mn1−O1 176.79(19) O5−Mn1−N2 94.4(2) O5−Mn1−N4 87.9(2) O8−Mn1−O1 89.8(2) O8−Mn1−O4 175.2(2) O8−Mn1−O5 93.4(2) O8−Mn1−N2 87.9(2) O8−Mn1−N4 88.7(2) N2−Mn1−N4 176.0(2)

* $\tau_4 = (360-(\alpha+\beta))/(360-2\times\arccos(-1/3))$, where α and β are the two largest bond angles at the metal centre. arccos(−1/3) is the tetrahedral angle ≈ 109.5 °.

Table S1. Geometric analysis of metal centres

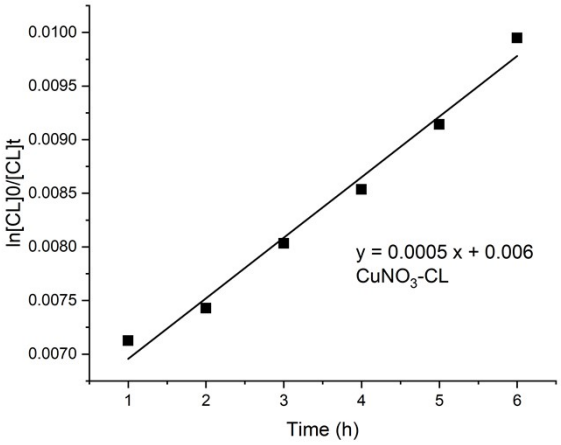

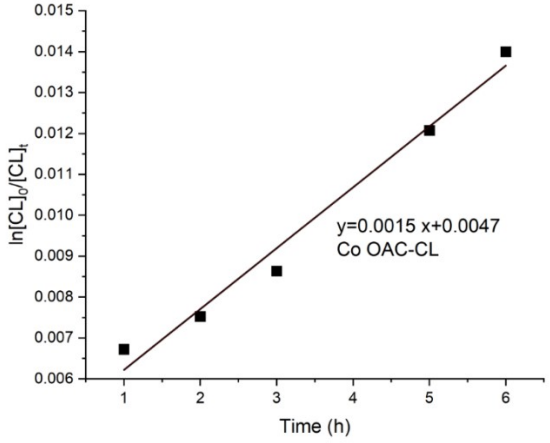

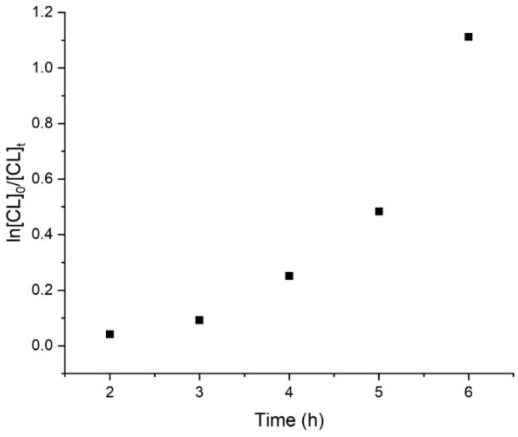

Figure S6, Individual kinetic graphs for PCL.

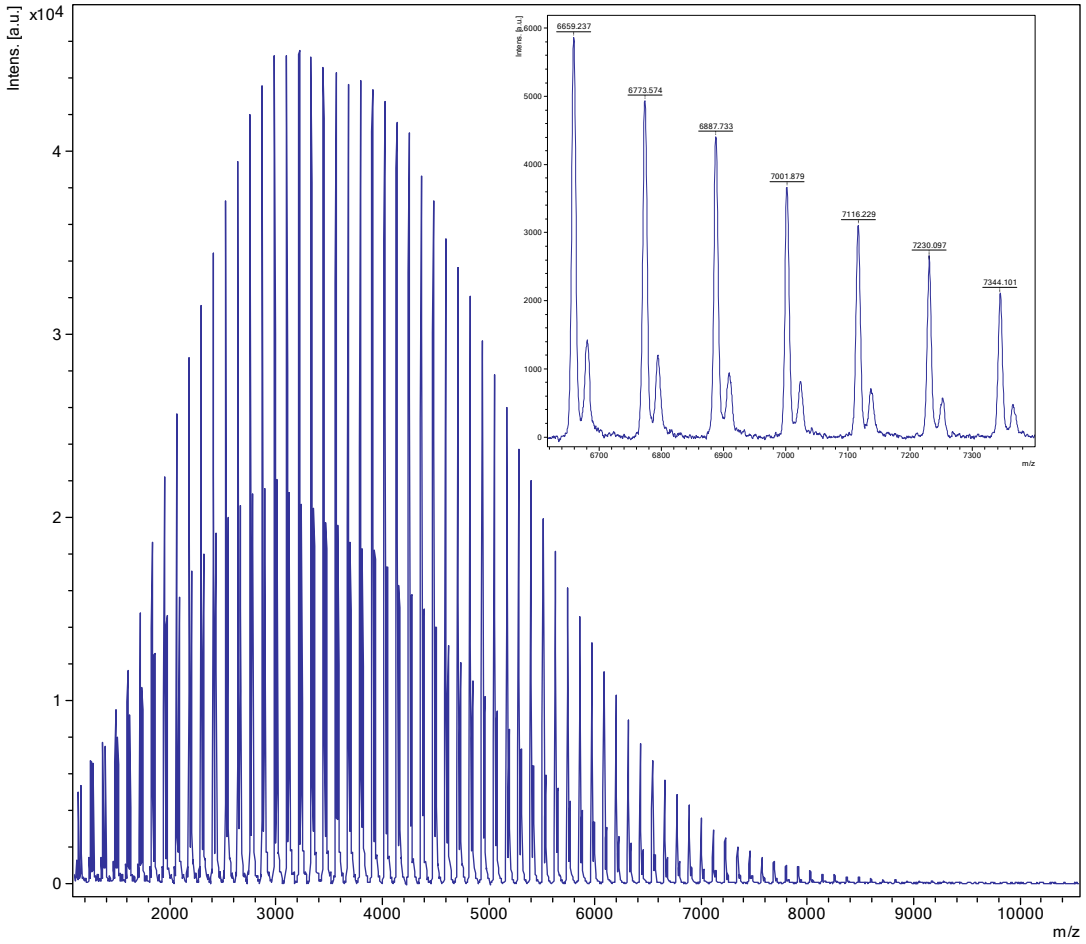

Figure S7. MALDI-ToF spectrum of PCL obtained from entry 1, table 1 (**1**, 500:1, melt, N_2). The main families are cyclic polymers as the potassium adducts [M = n x 114.14(CL) + 39.1 (K^+)] e.g., calc. 6887.5, n = 60, obsv. 6887.8 (this was also confirmed by ^{1}H NMR spectroscopy, Fig. S8, ESI).

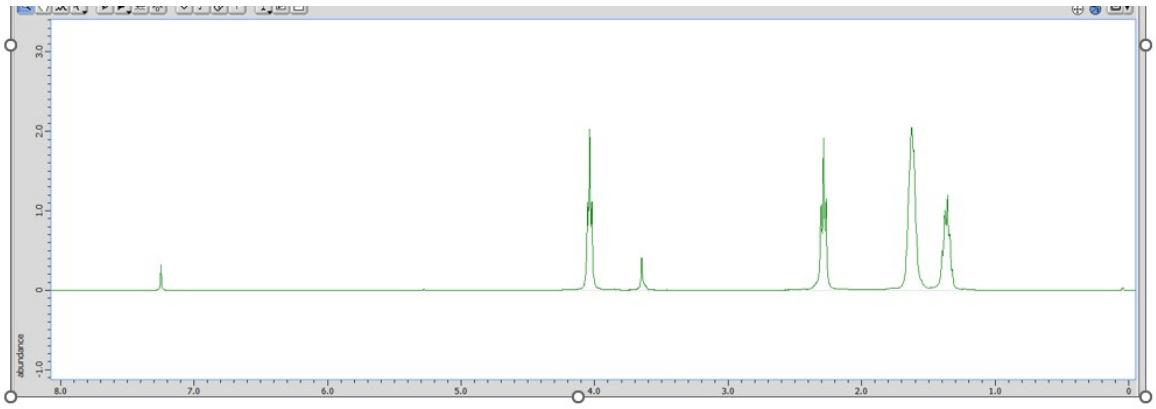

Figure S8. ^{1}H NMR spectrum of PCL obtained from entry 1, table 1.

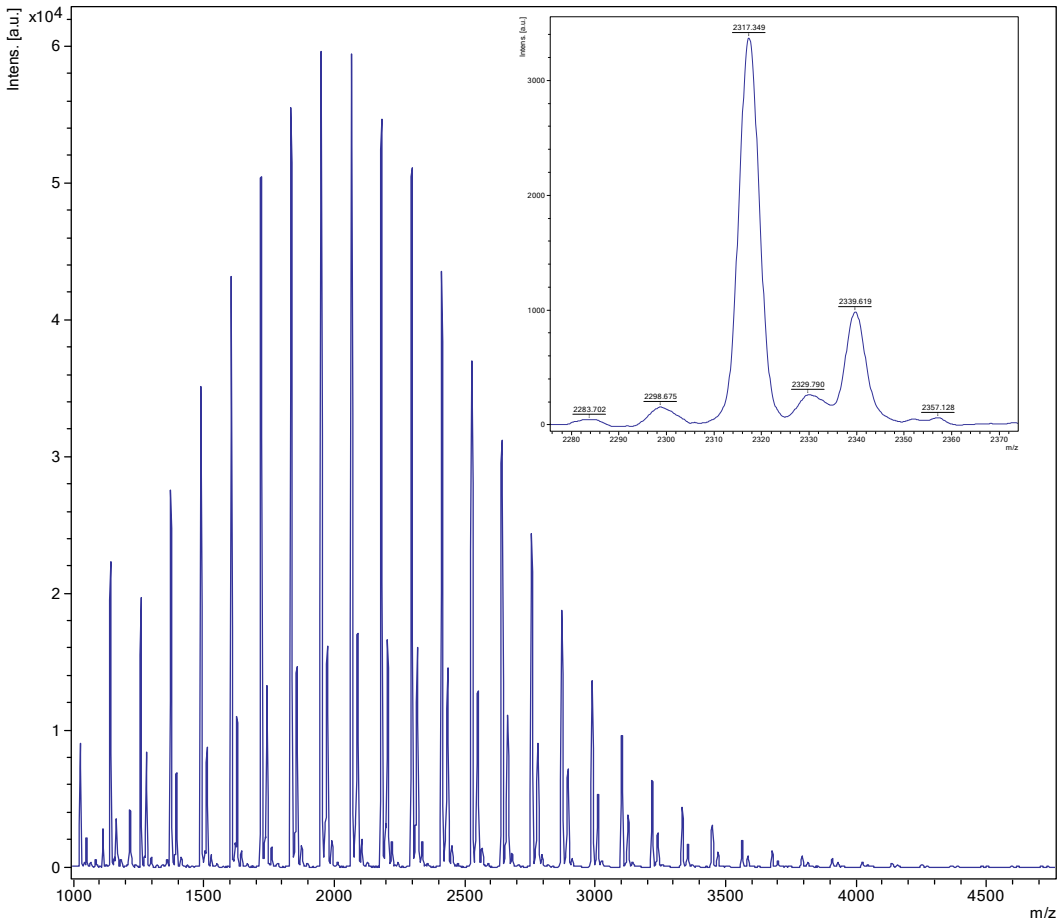

Figure S9. MALDI-ToF spectrum of PCL using **2** as a melt. MALDI-ToF spectrum of PCL obtained from entry 2, table 1 (**2**, 500:1, melt, N_2). The main families are i) chain polymer (terminated by 2 OH groups) as potassium adducts [M = 17 (OH) + 1(H) + n × 114.14 (CL) + 39.1 (K^+)] (e.g., for n = 20, calc. 2339.9 obsv. 2339.6; ii) cyclic polymers as the potassium adducts offset by *ca*. 4.6Da [M = n x 114.14(CL) + 39.1 (K^+)] e.g., calc. 2321.9, n = 20, obsv. 2317.3.

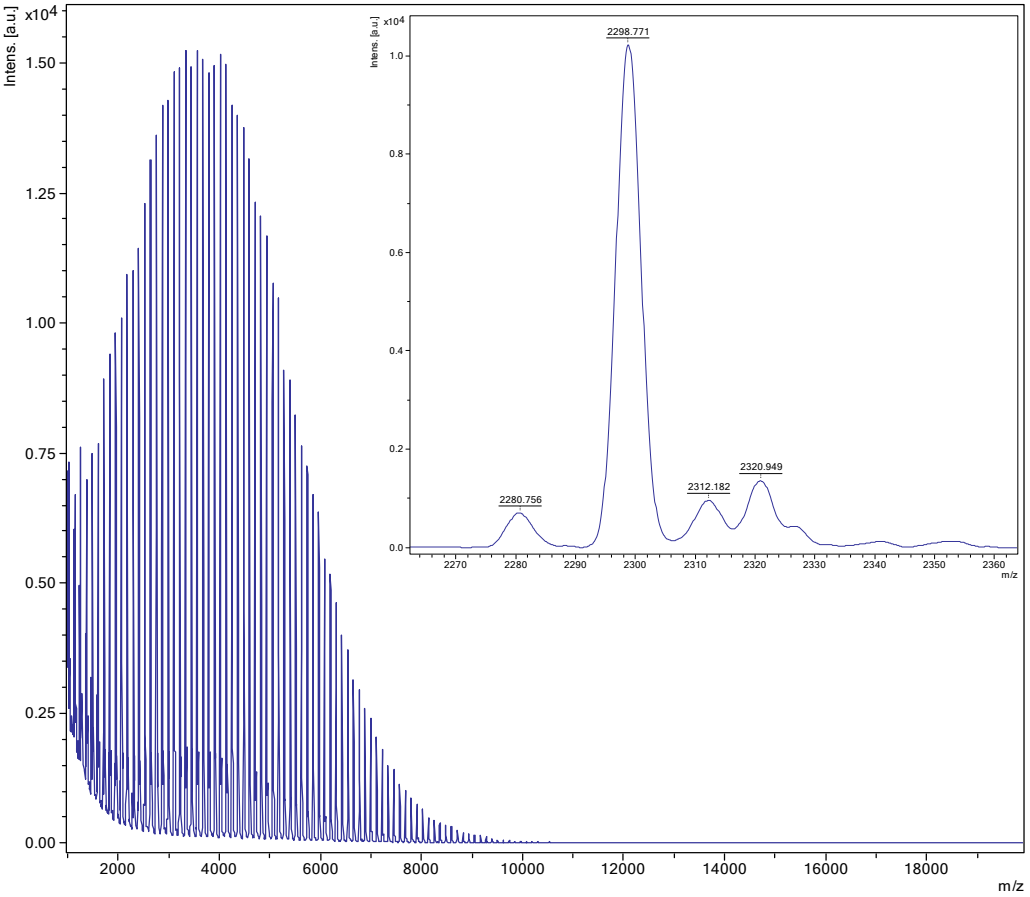

Figure S10. MALDI-ToF spectrum of PCL obtained from entry 4, table 1 (**3**, 500:1, melt, N_2). The major family of peaks are linear polymers with HO/H end group, e.g. n = 20, calc = 2300.8, obsv. = 2298.8. The minor families are cyclic polymers including the potassium adducts [M = n x 114.14(CL) + 39.1 (K^+)] e.g., calc. 2321.9, n = 20, obsv. 2320.9; n = 22, calc = 2550.2, obsv. 2551.2.

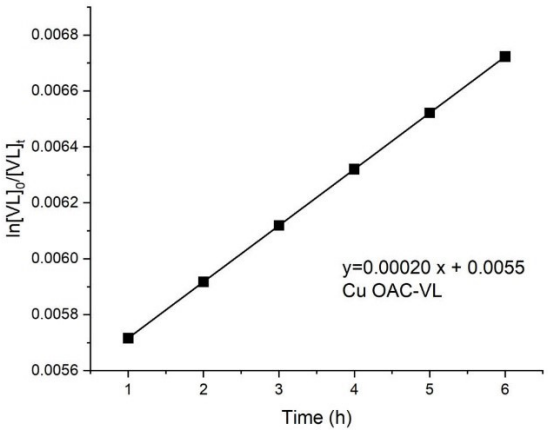

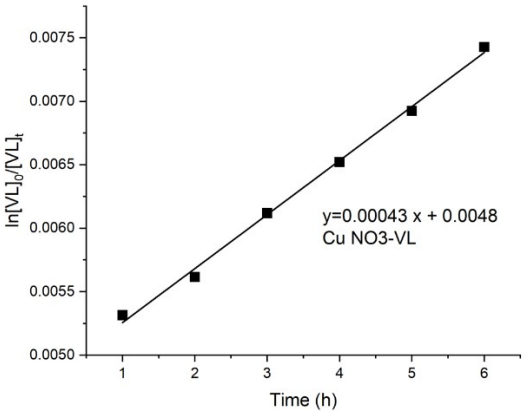

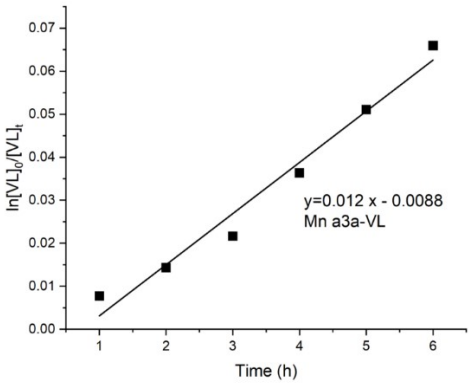

Figure S11, Individual kinetic graphs for PVL.

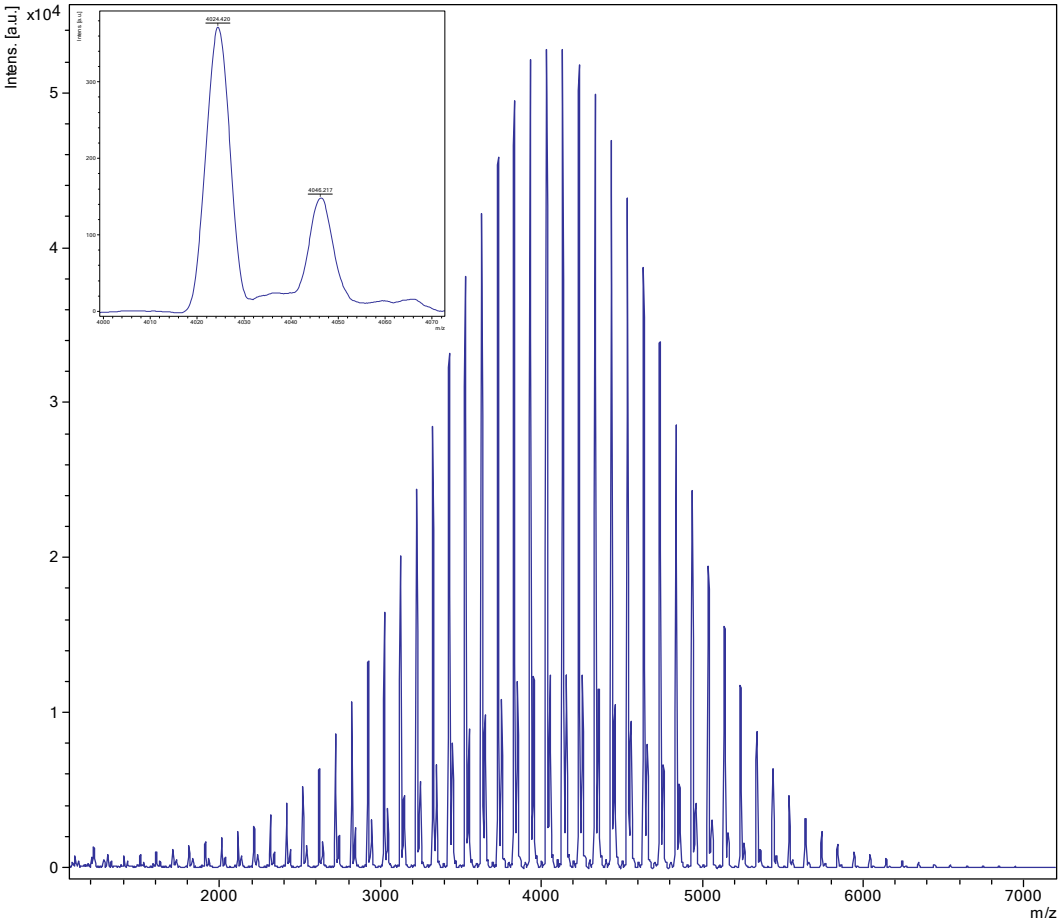

Figure S12. MALDI-ToF spectrum of PVL obtained from entry 6, table 1 (**1**, 500:1, melt, N_2). The main family is cyclic polymers as the sodium adducts [M = n x 100.12 (VL) + 22.99 (Na^+)] e.g., calc. 4027.8, n = 40, obsv. 4024.4. There is also a minor family with chain polymer (terminated by 2 OH groups) as sodium adducts [M = 17 (OH) + 1(H) + n × 100.12 (VL) + 22.99 (Na^+)] (e.g., for n = 40, calc. 4045.6 obsv. 4046.2.

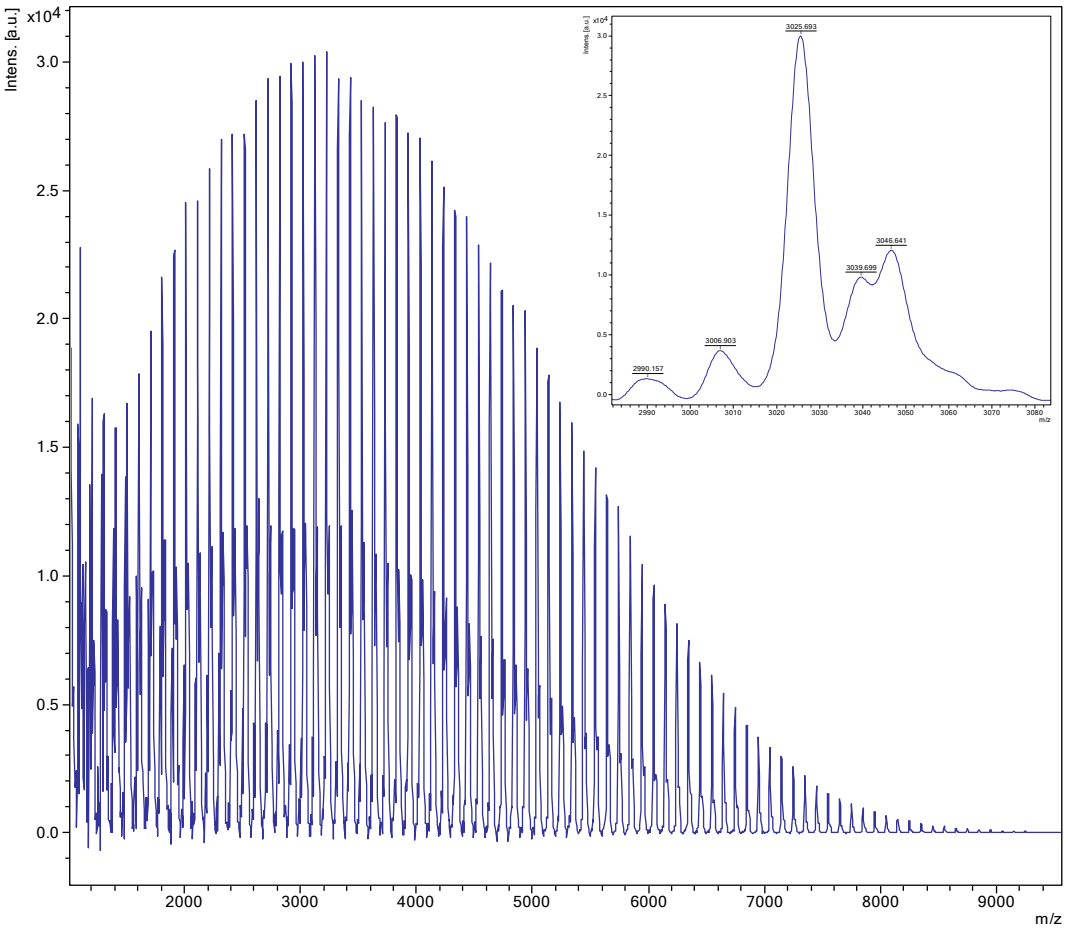

Figure S13. MALDI-ToF spectrum of PVL obtained from entry 9, table 1 (**3**, 500:1, melt, N_2). The main family is cyclic polymers as the sodium adducts [M = n x 100.12 (VL) + 22.99 (Na^+)] e.g., calc. 3026.6, n = 30, obsv. 3025.7. There is also a minor family with chain polymer (terminated by 2 OH groups) as sodium adducts [M = 17 (OH) + 1(H) + n × 100.12 (VL) + 22.99 (Na^+)] (e.g., for n = 30, calc. 3044.6 obsv. 3046.6.

For **1** (entry 1, Table 1):

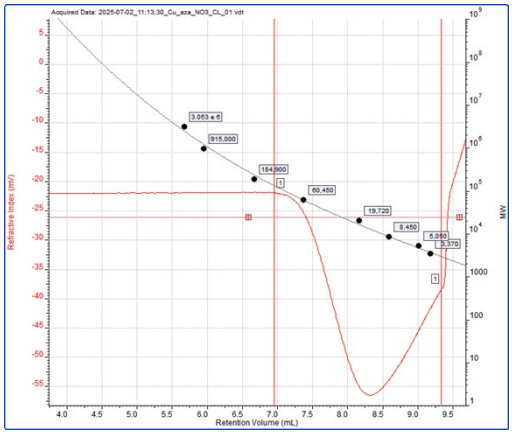

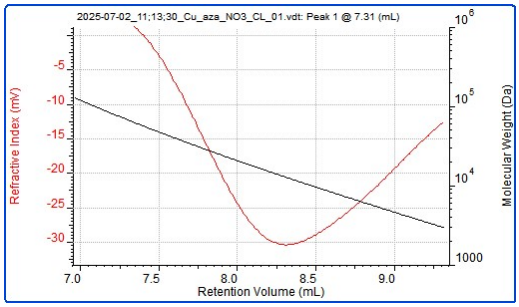

Peak 1

Ret Vol (mL) 7.305

*M*n (Da) 8,272

*M*w (Da) 10,304

*M*z (Da) -5551

*M*p (Da) 66,050

*M*w/*M*n 1.246

For **3** (entry 4, table 1):

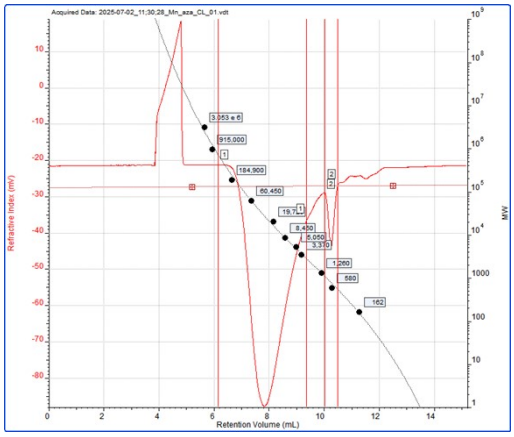

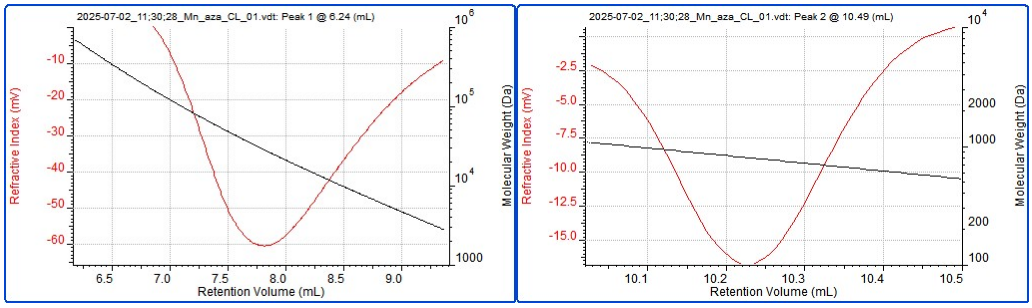

Peak	1	2
Ret Vol (mL)	6.243	10.491
*M*n (Da)	13,452	792
*M*w (Da)	13,760	804
*M*z (Da)	-397676	817
*M*p (Da)	586,640	536
*M*w/*M*n	1.023	1.015

Figure S14. Representative gpc traces for PCL

For **2** (Entry 8, Table 1):

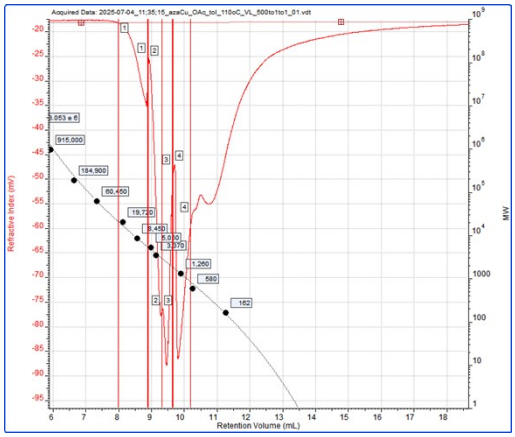

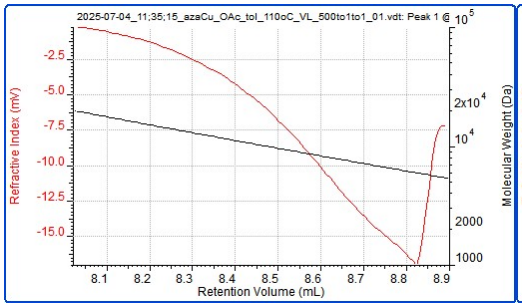

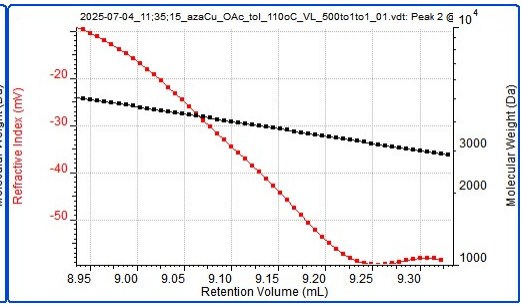

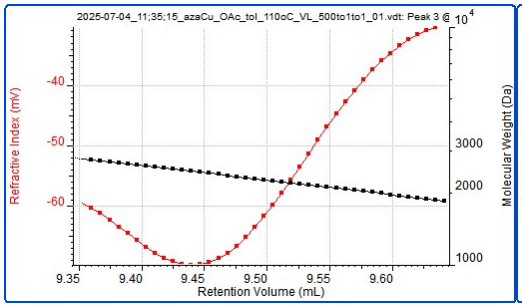

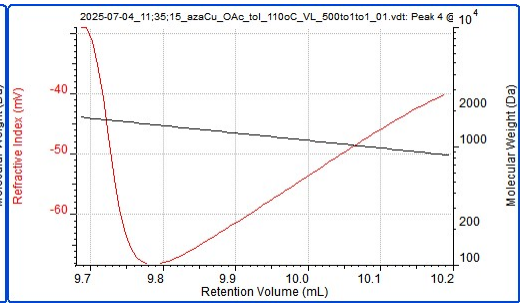

Peak	1	2	3	4
Ret Vol (mL)	8.026	8.936	9.634	9.687
*M*n (Da)	7,615	3,571	2,389	1,242
*M*w (Da)	8,231	3,650	2,419	1,297
*M*z (Da)	9,085	3,735	2,447	1,349
*M*p (Da)	19,535		5,057	1,875	1,740
*M*w/*M*n	1.081	1.022	1.012	1.044

Figure S15. Representative gpc traces for PVL

Coordination-insertion ROP mechanism

We note that both BnOH and H_2O are known to be efficient initiators [23],[S8] and given the monomers were not subject to purification (*i.e.* used as received) and that the ROPs were conducted under air, it is the HO/H end groups arise via H_2O as initiator as has been reported elsewhere [24].[S9] A typical mechanism is shown below.

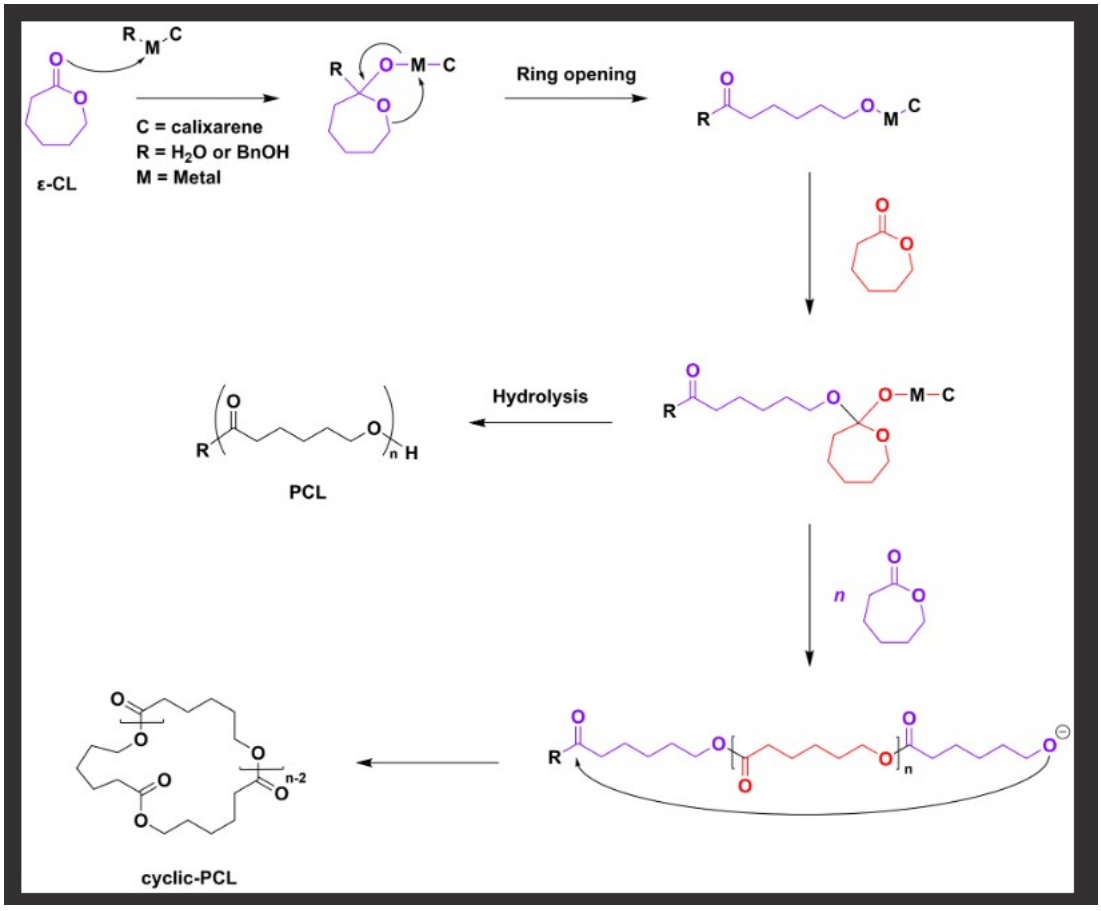

Comparison *versus* [Sn(Oct)$_2$]

For ε-CL, catalyst systems **1** and **3** (Table 1, entries 1 and 4) compare favourably with [Sn(Oct)$_2$] Table S2, entry 2) in terms of conversion rate and molecular weight (M_n), whilst performing with better control (Đ = 1.25 and 1.02 *versus* 1.94).

In solution, catalyst system **2** (Table 1, entry 3) outperforms [Sn(Oct)$_2$] (Table S2, entry 1) in terms of conversion and control, with the tin system exhibiting multimodal behaviour.

For δ-VL, in the absence of BnOH, only system **1** (Table 1, entry 6) competes with [Sn(Oct)$_2$] (Table S2, entry 3) in terms of conversion rate, whilst displaying better control (Đ 1.20 *versus* 2.15). Catalyst systems **2** (Table 1, entry 7) and particularly 3 (Table 1, entry 9) exhibit poorer conversion rates than [Sn(Oct)$_2$] (Table S2, entry 3) but comparable molecular weight (M_n) and better control (Đ = 1.17 and 1.08 *versus* 2.15).

Table S2. Comparison *versus* [Sn(Oct)$_2$] (all runs conducted under air at 130 °C)[S10]

Entry	[M]:[Cat]	Conv[a] (%)	$M_{n(obsv)}$[b]	M_n *corrected*[c]	$M_{n,Cal}$[d]	Đ[b]
1[e]	500 CL:1	56	10730/3440	6010/1930	31980	1.21/1.11
2[f]	500 CL:1	>99	10920	6120	56520	1.64
3[f]	500 VL:1	>99	6620	3770	49580	2.15

[a] Determined by ^{1}H NMR spectroscopy. [b] Measured by GPC in THF relative to polystyrene standards; [c] M_n calculated values after Mark–Houwink correction[S11]; M_n corrected = 0.56 (or 0.57 for δ-VL) × M_n obsd. [d] Calculated from ([CL or VL]$_0$/[cat]$_0$) × conv (%) × monomer molecular weight (M_{CL} = 1114.14 or M_{VL} = 100.12) + end groups (H/OH used in this case). [e] Conducted in toluene. [f] Conducted as a melt.

Cell viability assay

CellTiter 96® AQ$_{ueous}$ One Solution Cell Proliferation Assay (Promega, Southampton, UK) containing a tetrazolium compound [3-(4,5-dimethylthiazol-2-yl)-5-(3-carboxymethoxyphenyl)-2-(4-sulfophenyl)–2H-tetrazolium, inner salt; MTS] was used to determine cell viability. 100 µL of cells were seeded at 1-5x10^5 mL^{-1} into clear 96-well plates. Cells were incubated for 72 h at 37 C in a 95 %/5% air/CO_2-humidified environment with different concentrations of the compounds. 10 µL of MTS reagent was added to each well and incubated for 4 h at 37 C. A FLUOstar Optima Fluorometer using Optima software (BMG Labtech) was used at an absorbance of 490 nm to detect the quantity of the coloured formazan product.

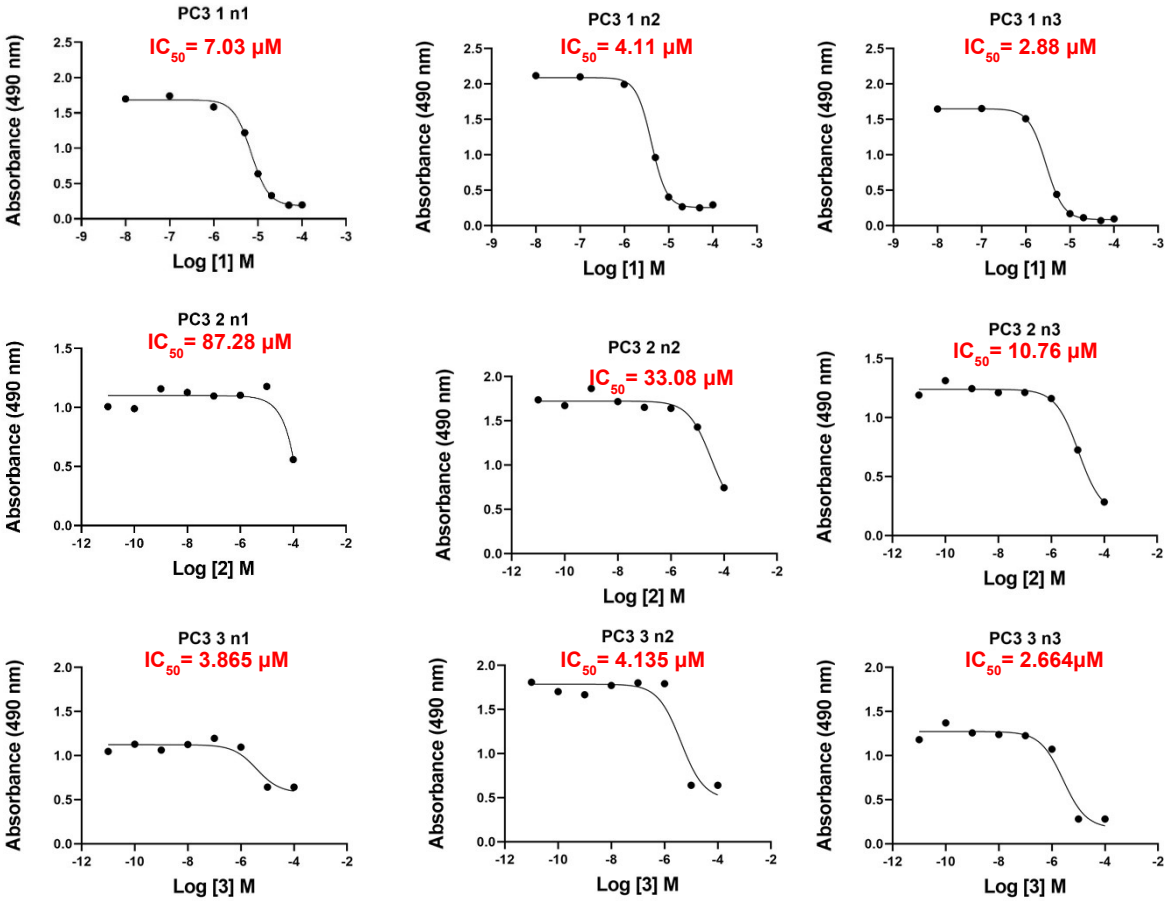

Figure S16. Cytotoxicity studies of **1** – **3** using PC3 cell lines.

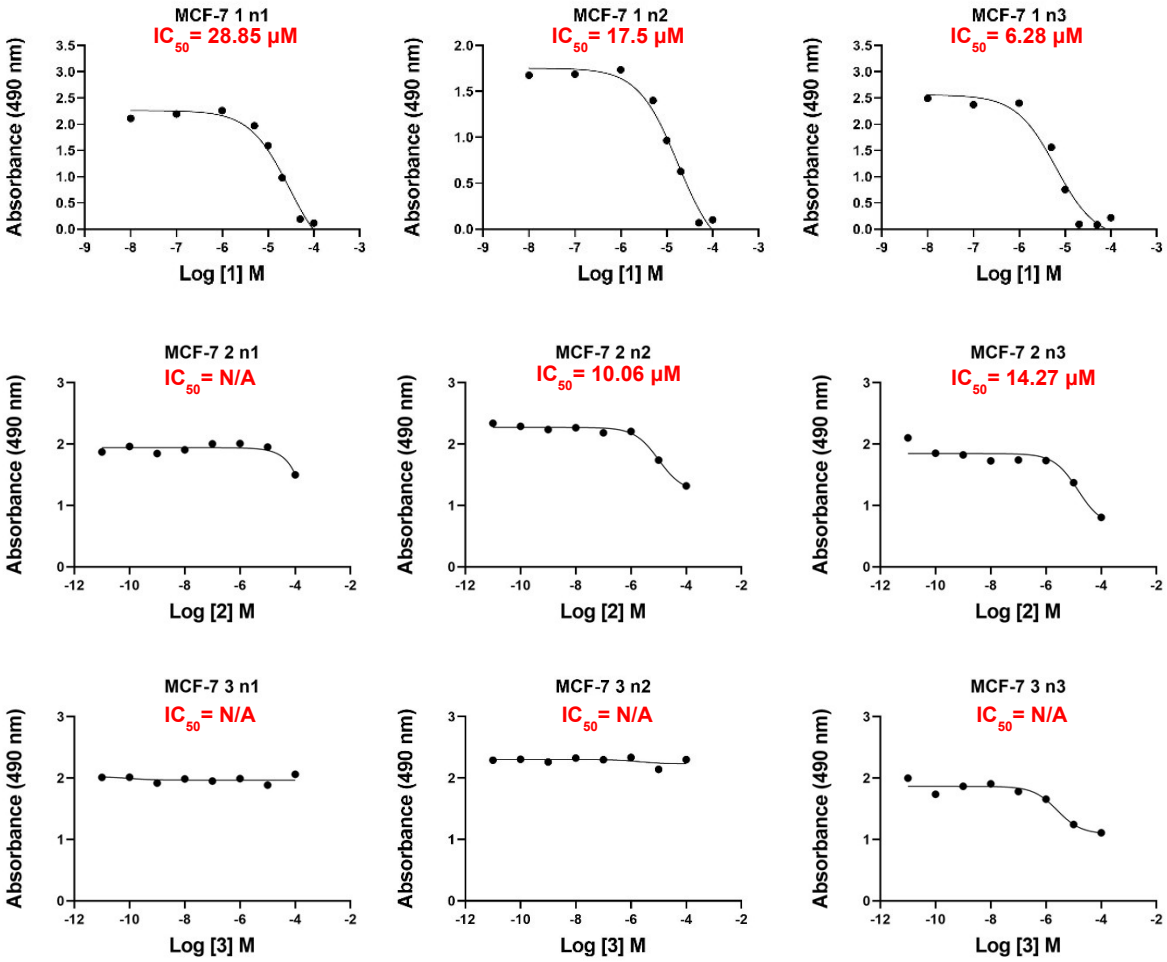

Figure S17. Cytotoxicity studies of **1** – **3** in MCF-7 cells. Individual concentration response curves of MCF-7 cells treated with **1** – **3** for 72 h. Cytotoxicity was measured via MTS assay.

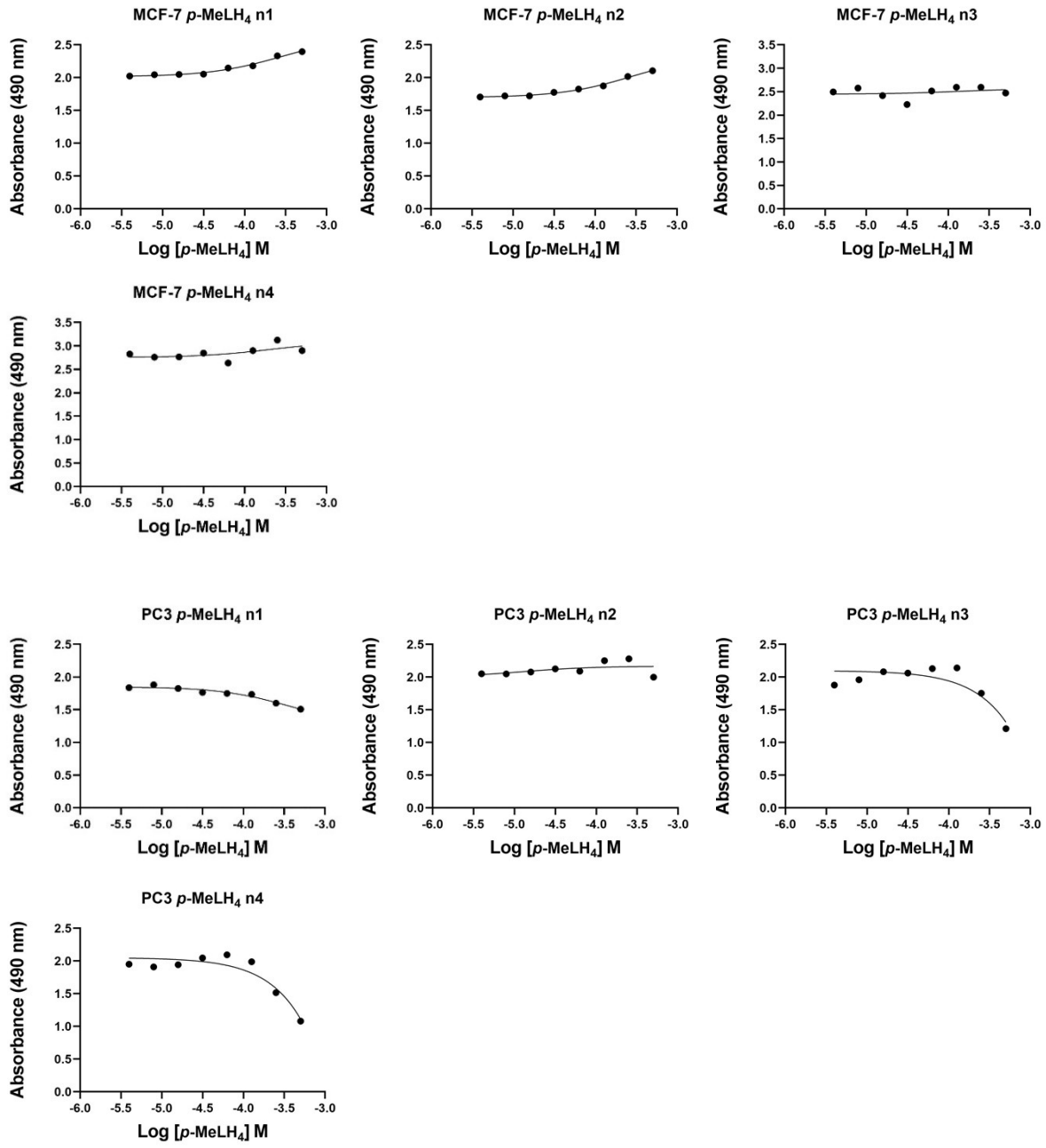

Figure S18. Cytotoxicity studies of *p*-MeLH$_4$ in MCF-7 and PC-3 cells. Individual concentration response curves of MCF-7 and PC-3 cells treated with *p*-MeLH$_4$ for 72 h. Cytotoxicity was measured via MTS assay.

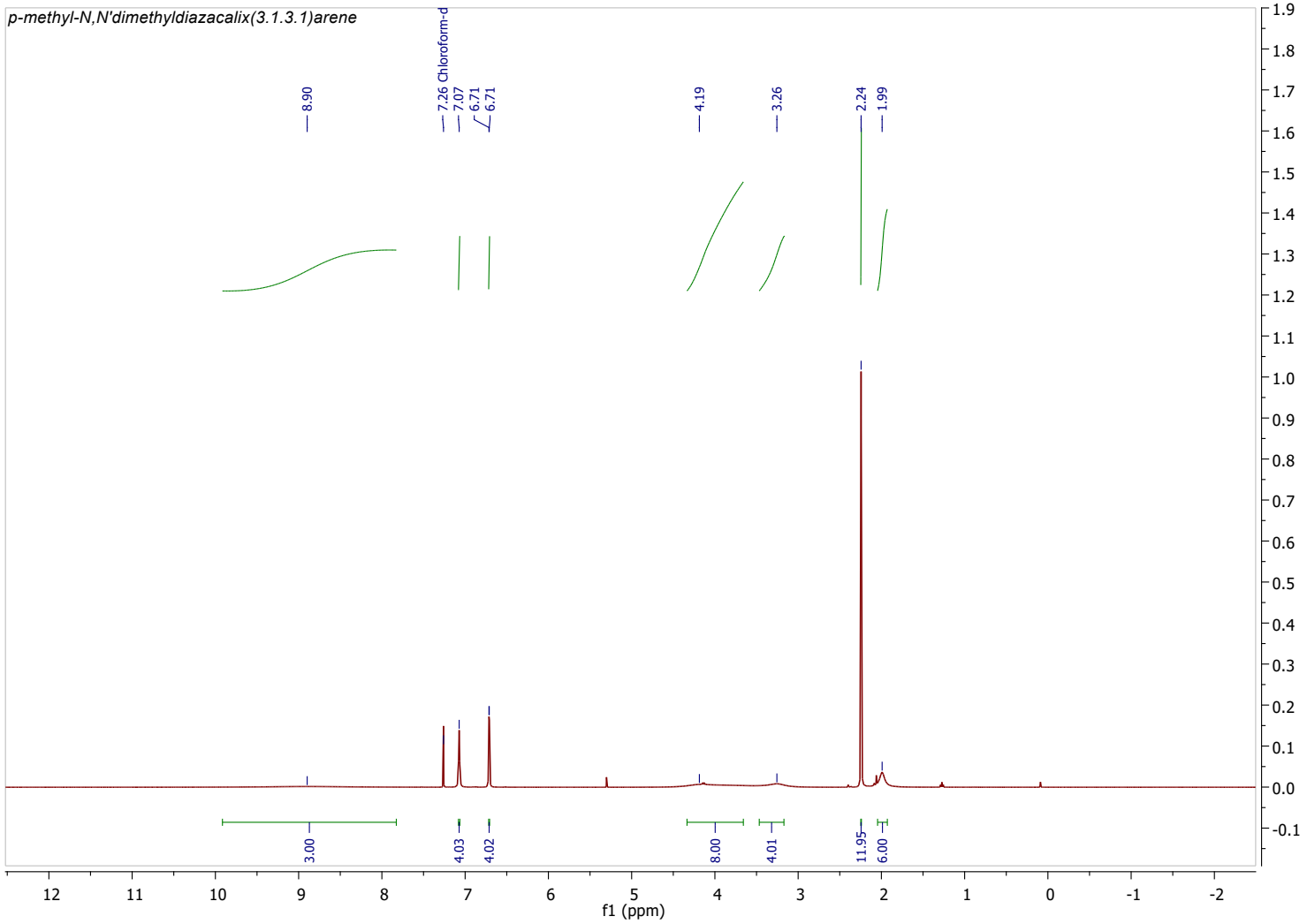

Figure S19. ^{1}H NMR spectrum of **L^{1}H$_{4}$** (298K, $CDCl_3$, 400 MHz).

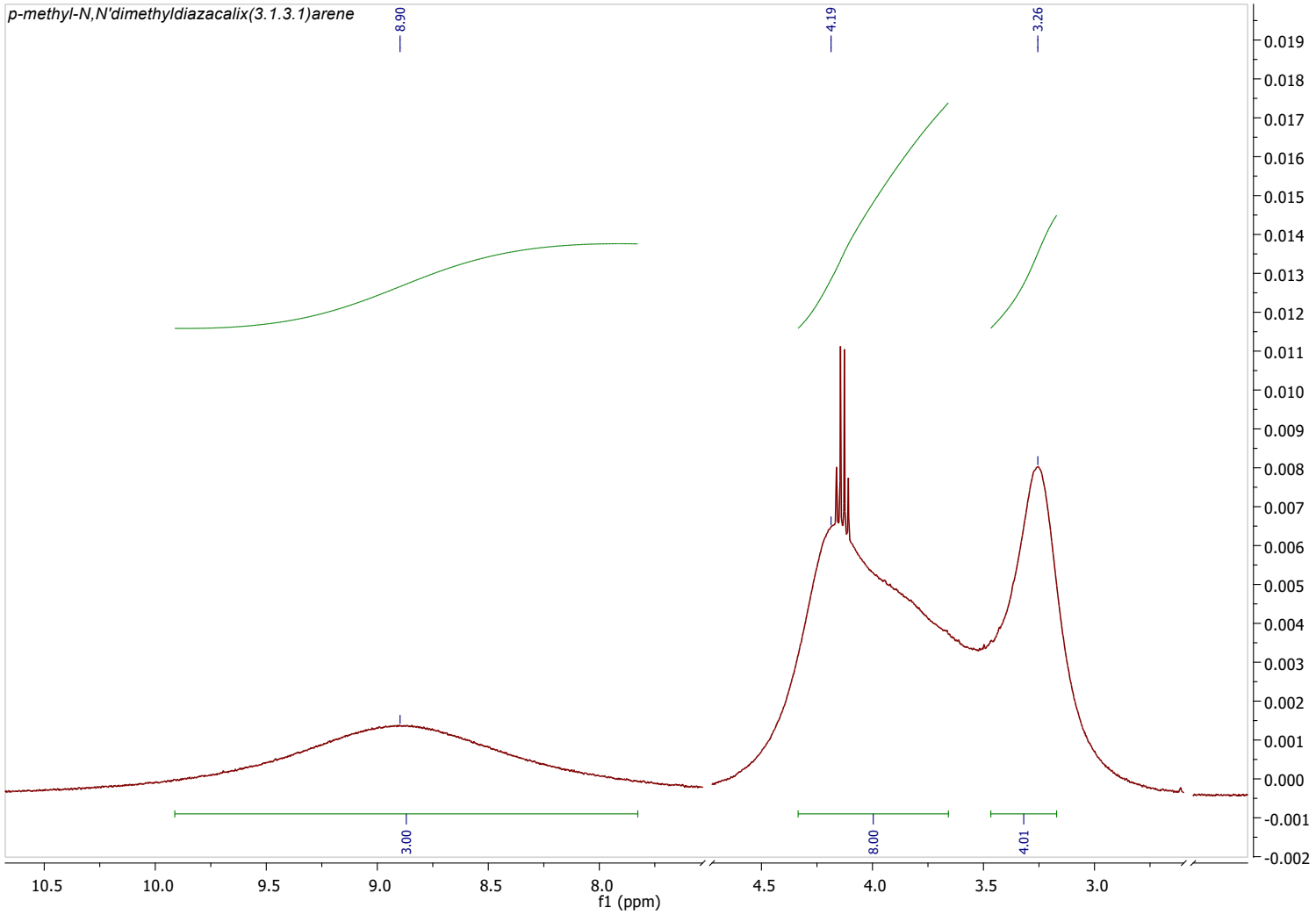

Figure S20. Expansions of the ^{1}H NMR spectrum of **L^{1}H$_{4}$** (298K, $CDCl_3$, 400 MHz). *Quartet at δ = 4.14 ppm is attributed to EtOAc*.

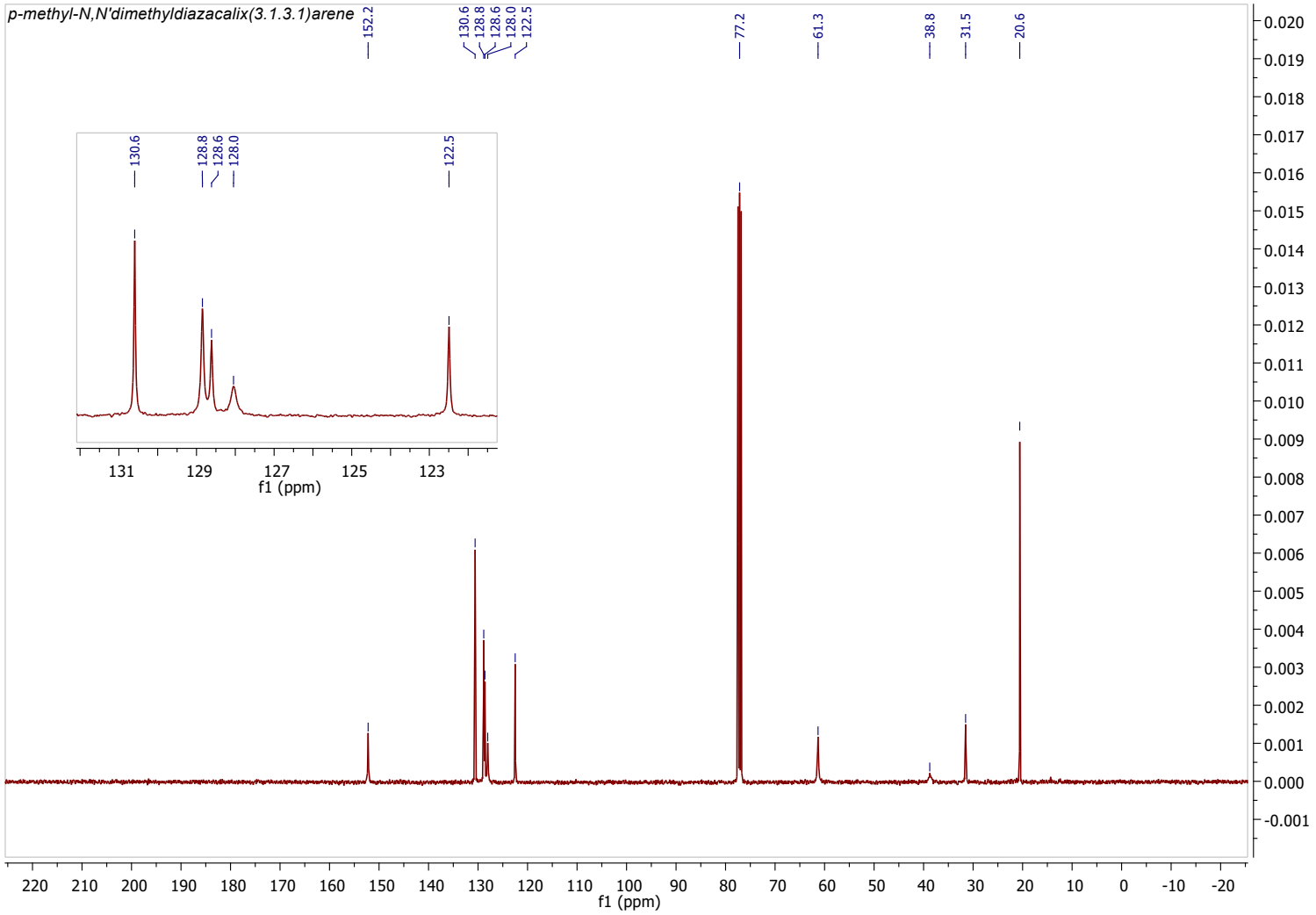

Figure S21. $^{13}C\{^{1}H\}$ NMR spectrum of **$L^{1}H_4$** (298K, $CDCl_3$, 101 MHz).

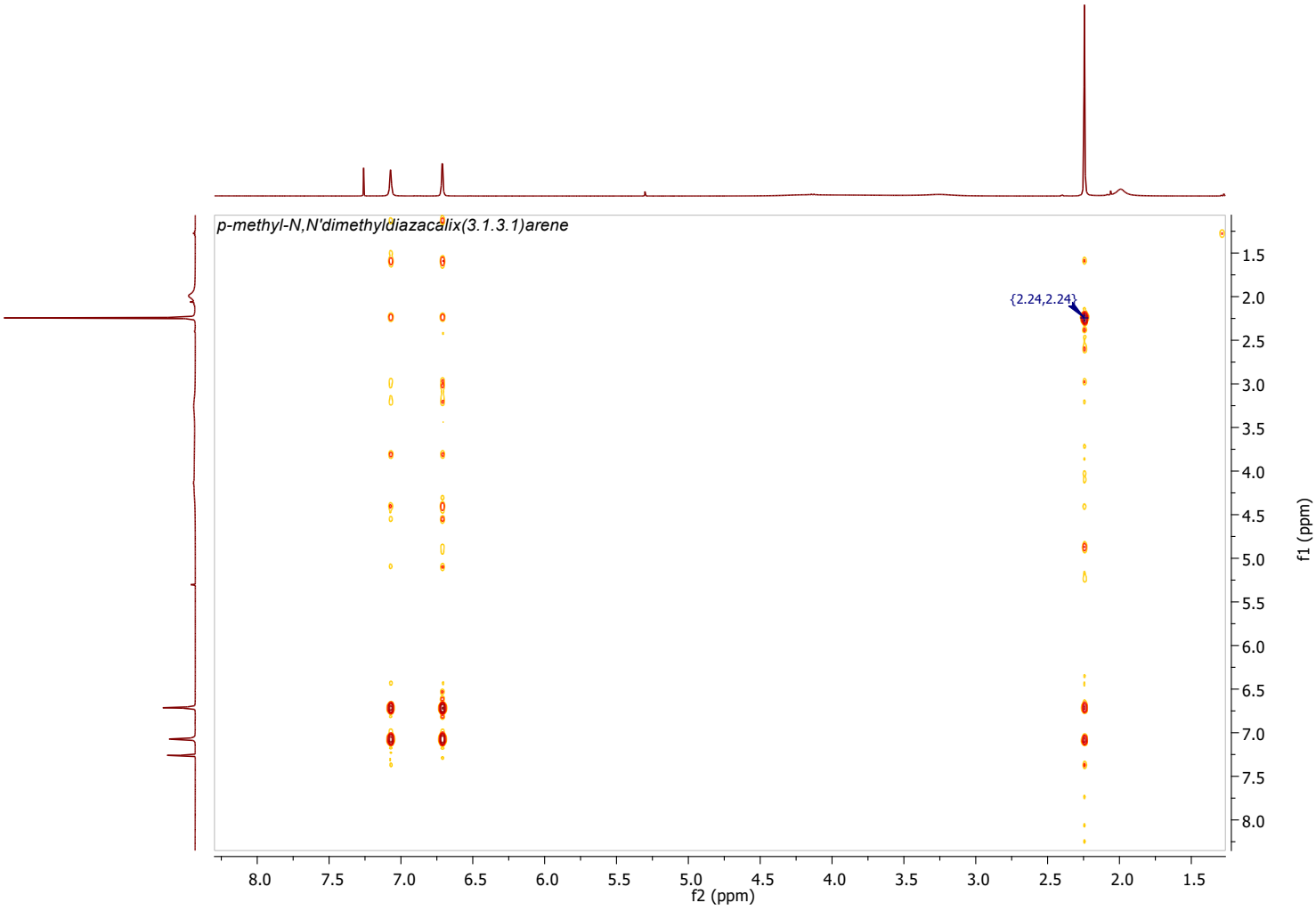

Figure S22. ^{1}H–^{1}H COSY NMR spectrum of **L^{1}H$_4$** (298K, $CDCl_3$). *Indicated resonances (blue) were used to align spectra and correlations.*

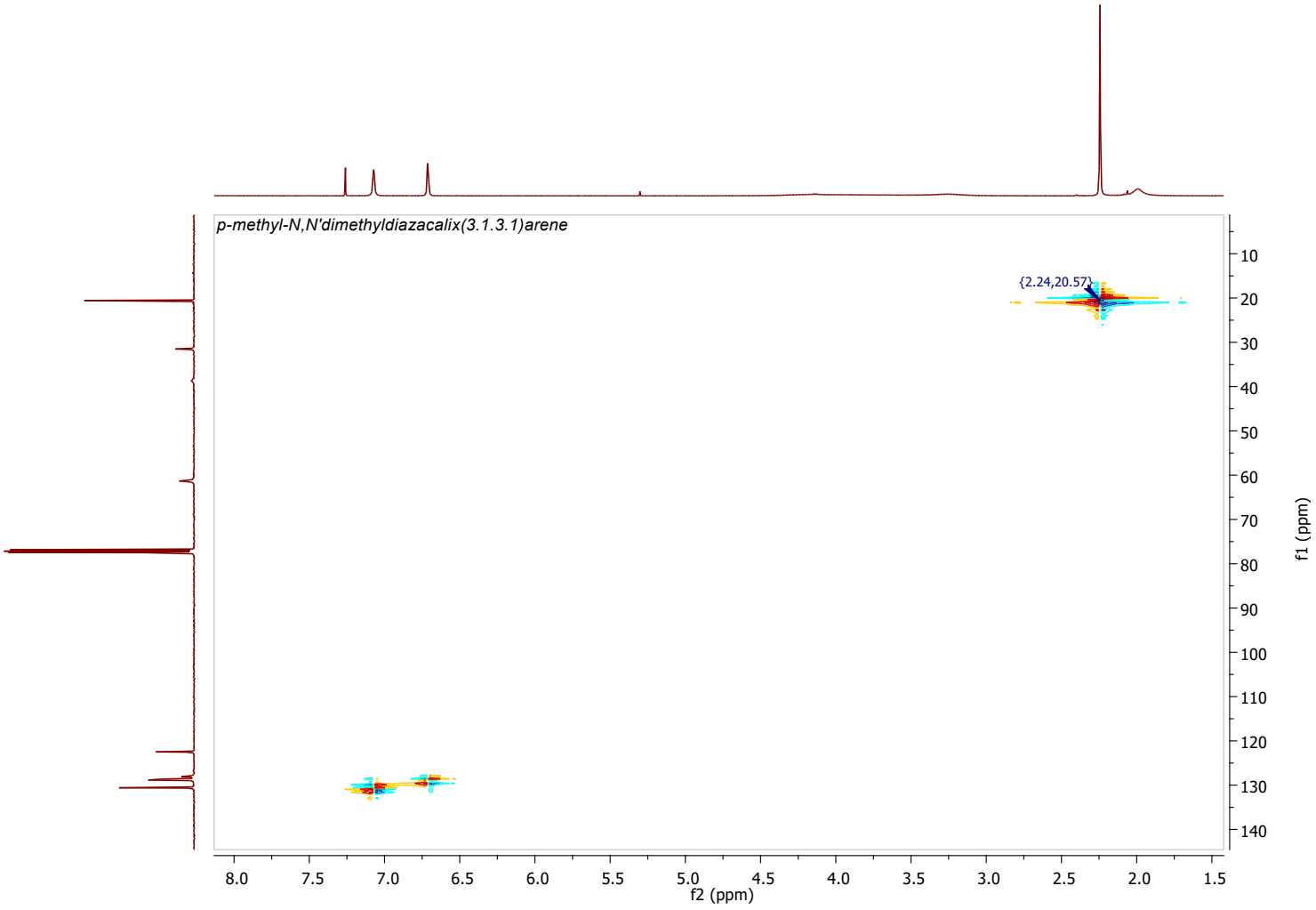

Figure S23. $^{1}H–^{13}C$ HSQC NMR spectrum of **$L^{1}H_{4}$** (298K, $CDCl_3$). *Indicated resonances (blue) were used to align spectra and correlations.*

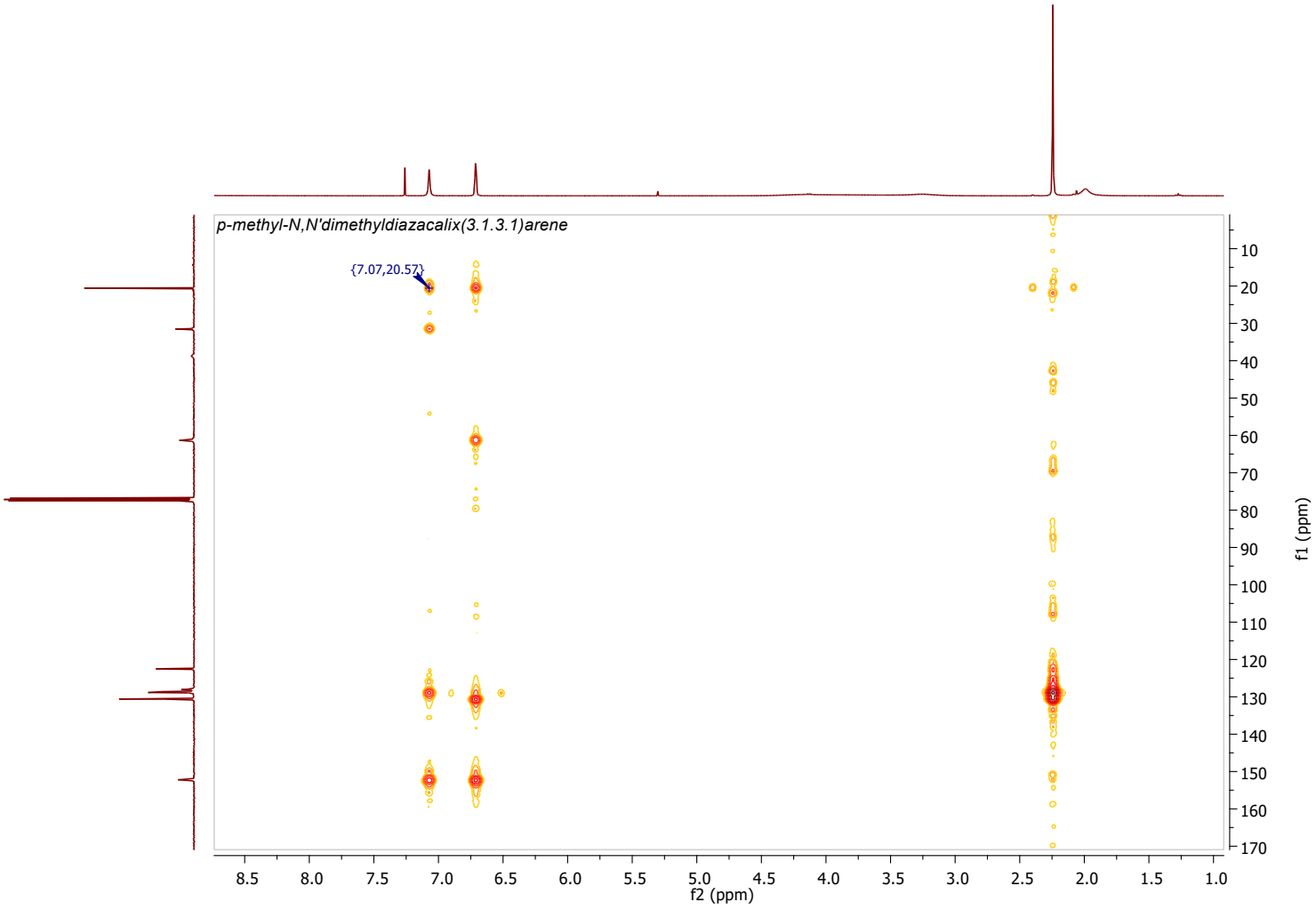

Figure S24. $^{1}H–^{13}C$ HMBC NMR spectrum of **L^{1}H$_4$** (298K, $CDCl_3$). *Indicated resonances (blue) were used to align spectra and correlations.*

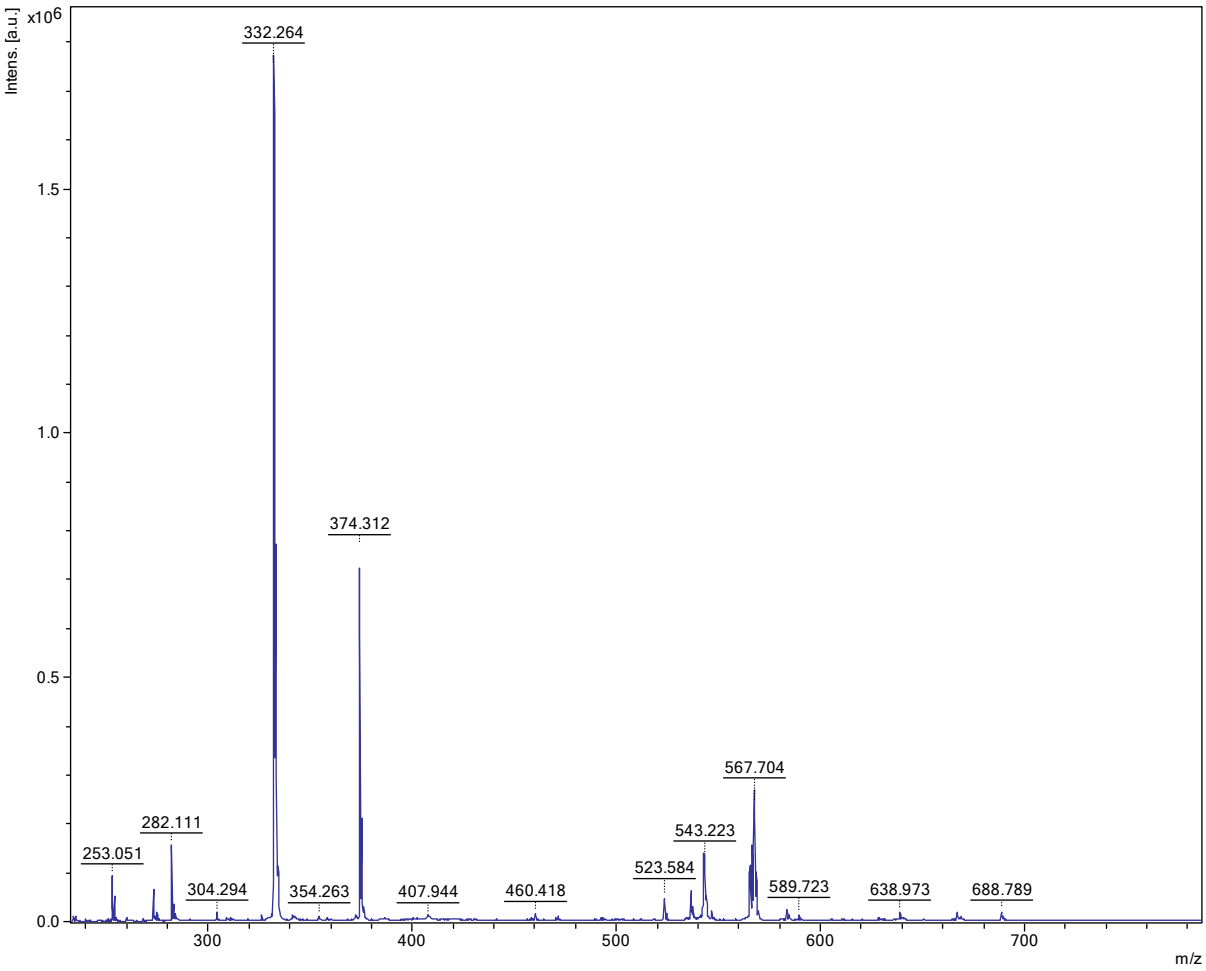

Figure S25: MS (MALDI-ToF) for **L^1H_4**.

566.713 as [M^+]; 567.704 as [MH^+]; 589.723 as [M^++ Na]; 638.97 as [M^+] + THF.

Matrix Assisted Laser Desorption/Ionization Time of Flight (MALDI-TOF) mass spectrometry was performed in a Bruker autoflex III smart beam in linear mode, and the spectra were acquired by averaging at least 100 laser shots. 2,5-Dihydroxybenzoic acid was used as the matrix and THF as solvent. Sodium chloride was dissolved in methanol and used as the ionizing agent. The sample was prepared by mixing 20 µl of matrix solution in THF (2 $mg \cdot mL^{-1}$) with 20 µL of matrix solution (10 $mg \cdot mL^{-1}$) and 1 µL of a solution of ionizing agent (1 $mg \cdot mL^{-1}$). Then 1 mL of these mixtures was deposited on a target plate and allowed to dry in air at ambient temperature.

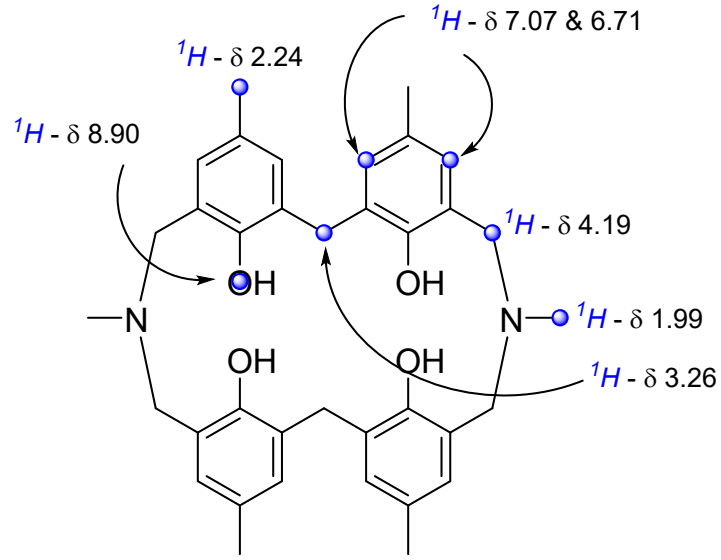

Figure S26. ^{1}H NMR assignments of **L^{1}H$_4$** (298K, $CDCl_3$). *Assignments made via 2D spectroscopies exhibited vide supra*.

Due to the broadness/diffuse nature of the resonances observed for ArCH_2Ar and NCH_2Ar peaks, no correlations could be determined in ^{1}H–^{1}H COSY, ^{1}H–^{13}C HSQC, or ^{1}H–^{13}C HMBC experiments. Thus, we have been unable to unambiguously assign the differing Ar-*H* resonances. Differing proton environments are represented as blue spheres.

Our analytical data for **L^{1}H$_4$**

^{1}H NMR (298 K, $CDCl_3$, 400 MHz): δ = 8.90 (br. s., 4H, -O*H*), 7.07 (s, 4H, Ar-*H*), 6.71 (d, *J* = 1.4 Hz, Ar-*H*), 4.19 (br. s. 8H, NCH_2Ar), 3.26 (br. s., 4H, ArCH_2Ar), 2.24 (s, 12H, ArCH_3), 1.99 (br. s., 6H, NCH_3) ppm.

^{13}C{^{1}H} NMR (298 K, $CDCl_3$, 101 MHz): δ = 152.2, 130.6, 128.8, 128.6, 128.0, 122.5, 61.3, 38.8, 31.5, 20.6 ppm.

MS (MALDI-TOF): Calcd for $C_{36}H_{43}N_2O_4$ = 567.322, found 567.704, $[M+H]^+$

ATR-FT-IR: 3170, 2911, 2864, 1922, 1739, 1602, 1475, 1433, 1382, 1336, 1317, 1298, 1242, 118, 1154, 1126, 1030, 965, 954, 903, 912, 870, 860, 843, 788, 772, 741, 688, 664, 643 cm^{-1}

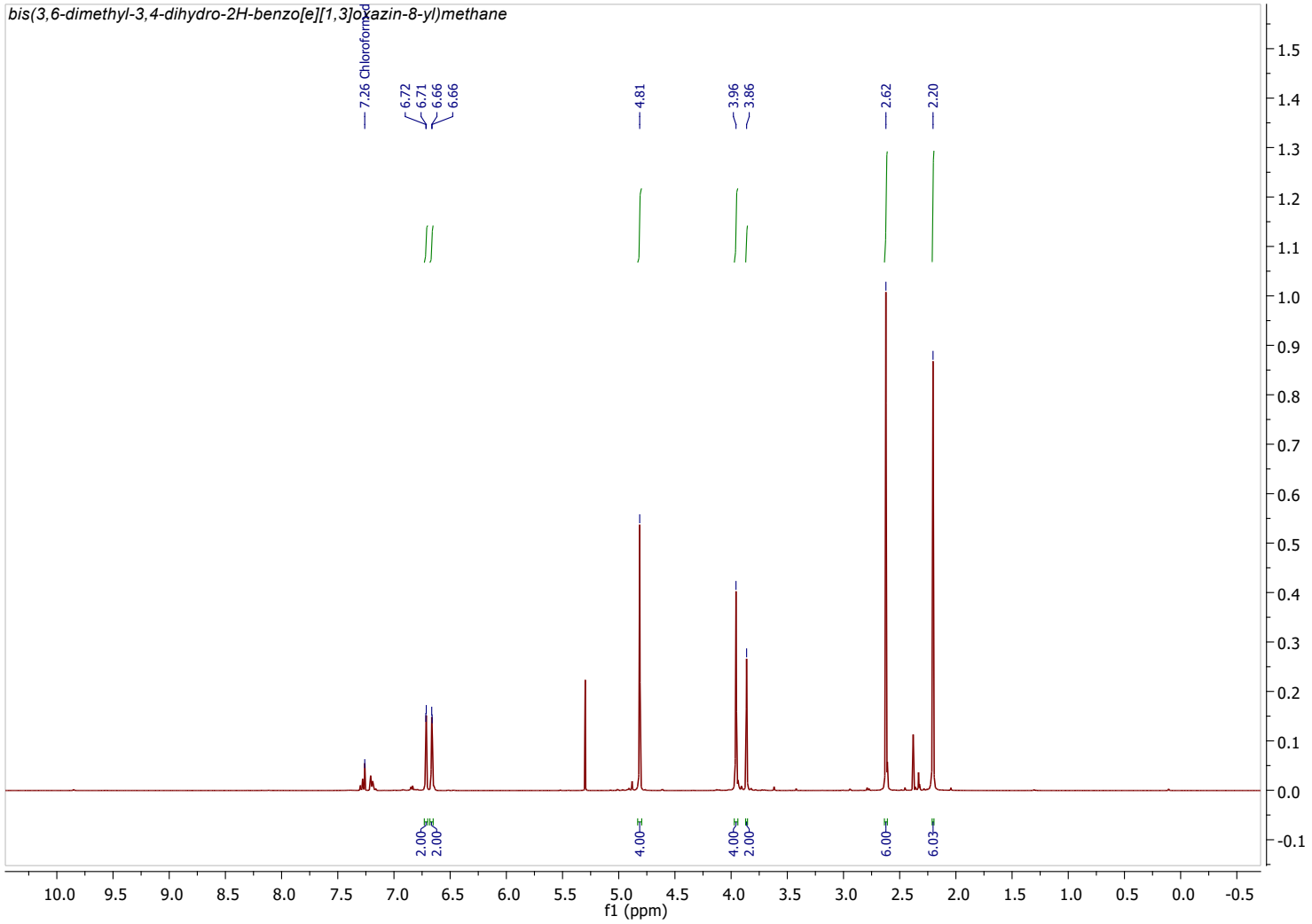

Figure S27. ^{1}H NMR spectrum of crude dihydrobenzoxazine **B** (298K, $CDCl_3$, 400 MHz).

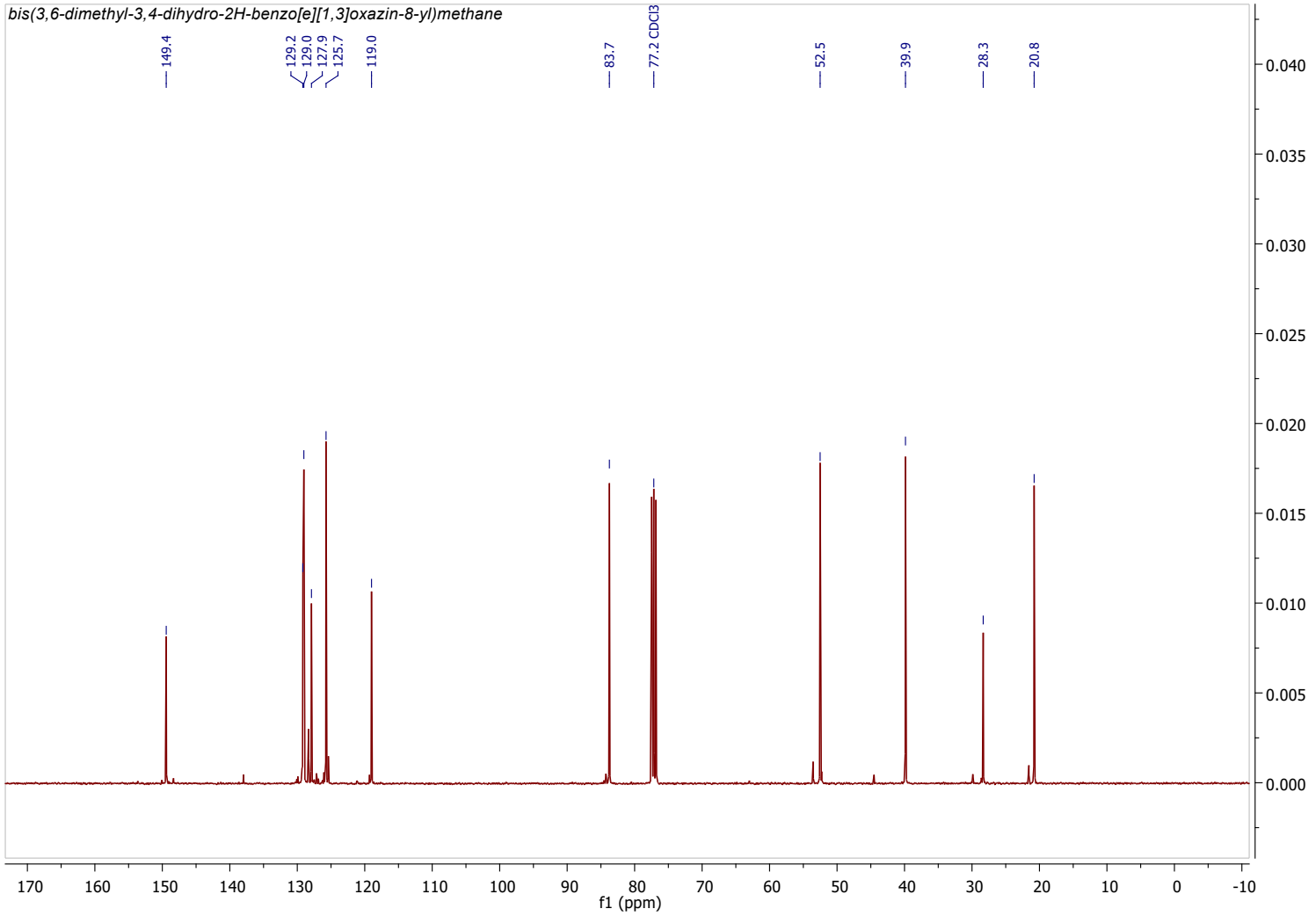

Figure S28. $^{13}C\{^{1}H\}$ NMR spectrum of crude dihydrobenzoxazine **B** (298K, $CDCl_3$, 101 MHz).

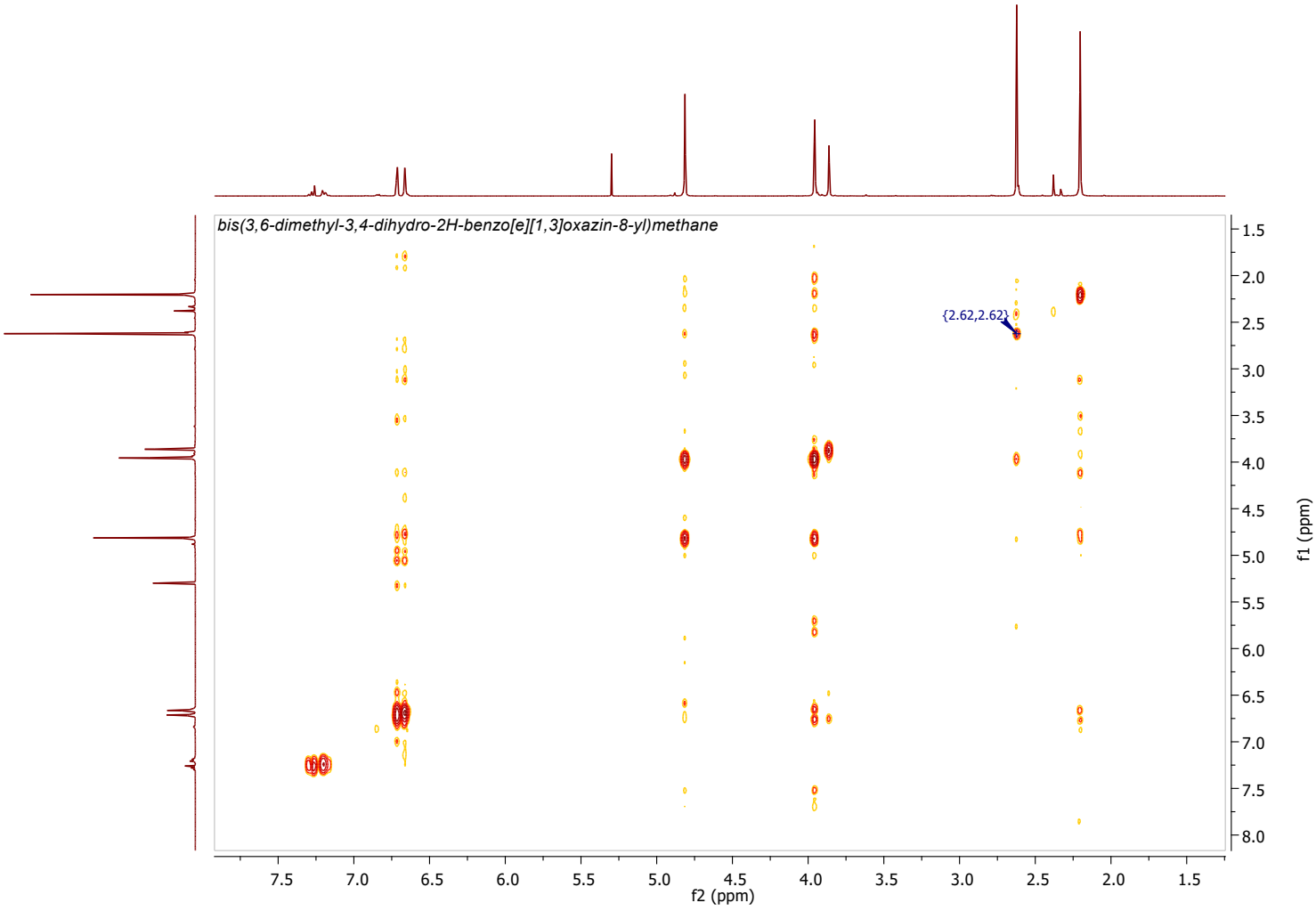

Figure S29. ^{1}H–^{1}H COSY NMR spectrum of dihydrobenzoxazine **B** (298K, $CDCl_3$). *Indicated resonances (blue) were used to align spectra and correlations.*

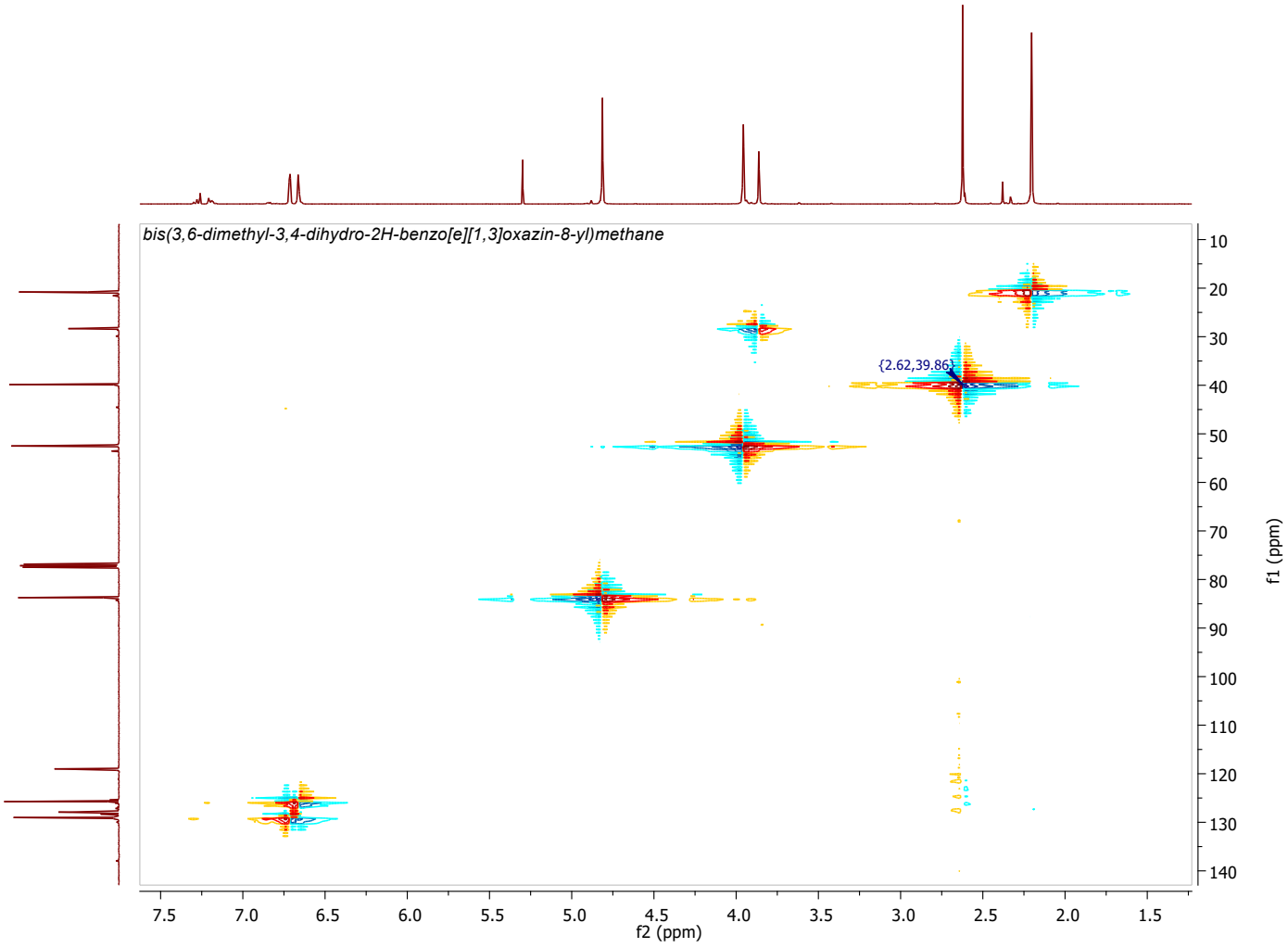

Figure S30. $^{1}H–^{13}C$ HSQC NMR spectrum of dihydrobenzoxazine **B** (298K, $CDCl_3$). *Indicated resonances (blue) were used to align spectra and correlations.*

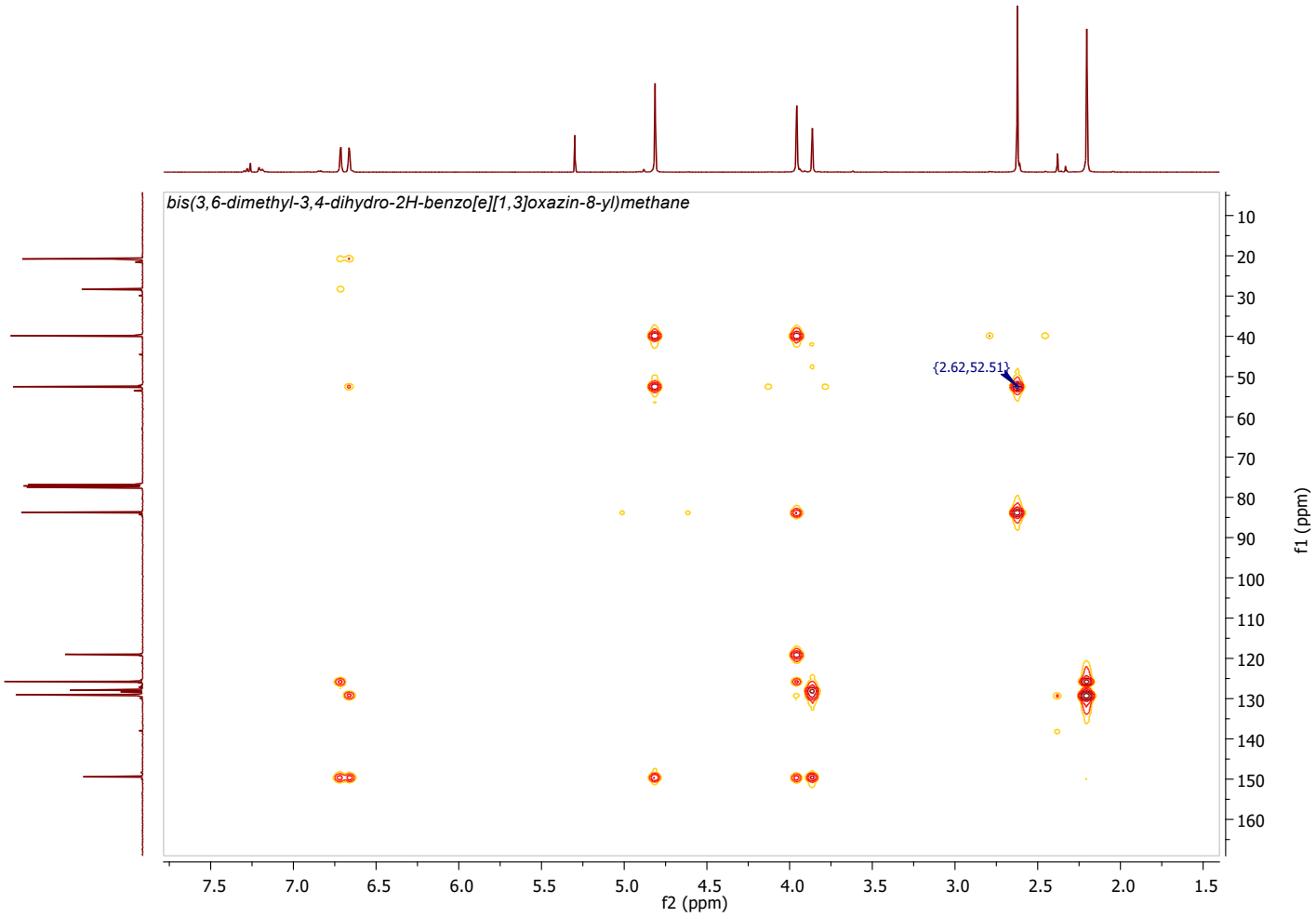

Figure S31. $^{1}H–^{13}C$ HMBC NMR spectrum of dihydrobenzoxazine **B** (298K, $CDCl_3$). *Indicated resonances (blue) were used to align spectra and correlations.*

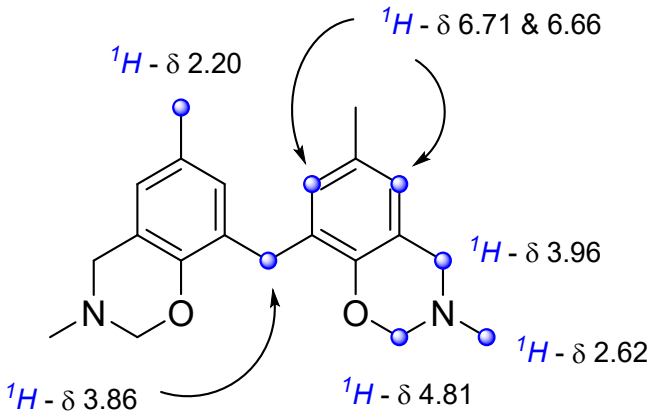

Figure S32. ^{1}H NMR assignments of dihydrobenzoxazine **B** (298K, $CDCl_3$). *Assignments made via 2D spectroscopies exhibited vide supra*.

^{1}H NMR ($CDCl_3$, 400 MHz, 298 K): δ = 6.71 (d, *J* = 1.5 Hz, 2H), 6.66 (d, *J* = 1.3 Hz, 2H), 4.81 (s, 4H), 3.96 (s, 4H), 3.86 (s, 2H), 2.62 (s, 6H), 2.20 (s, 6H) ppm.

^{13}C NMR ($CDCl_3$, 101 MHz, 298 K): δ =149.4, 129.2, 129.0, 127.9, 125.7, 119.0, 83.7, 52.5, 39.9, 28.3, 20.8 ppm.

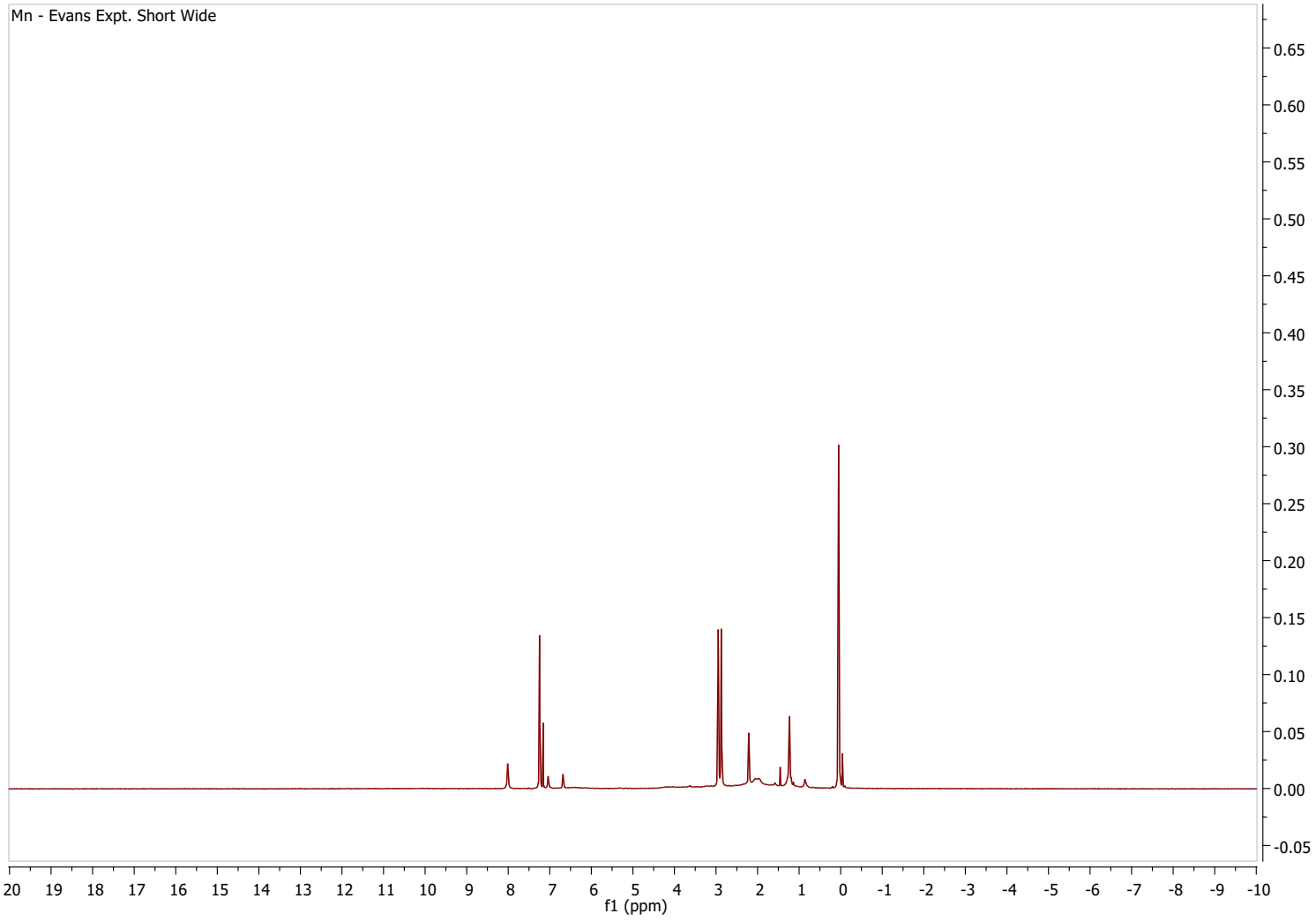

Figure S33. ^{1}H NMR spectrum of complex **3** (Mn) (298K, $CDCl_3$, 400 MHz).

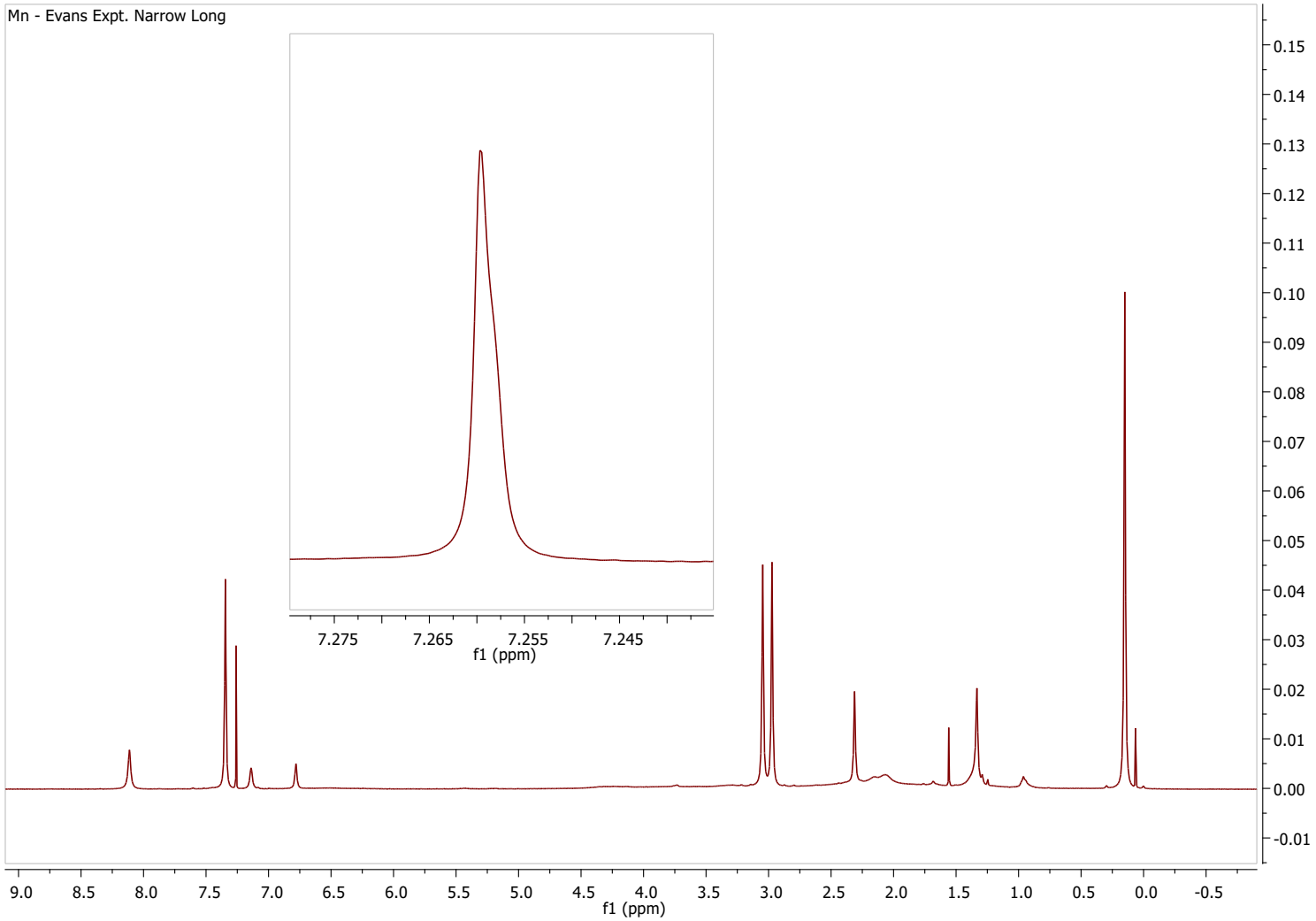

Figure S34. ^{1}H NMR spectrum of complex **3** (Mn) (298K, $CDCl_3$, 400 MHz).

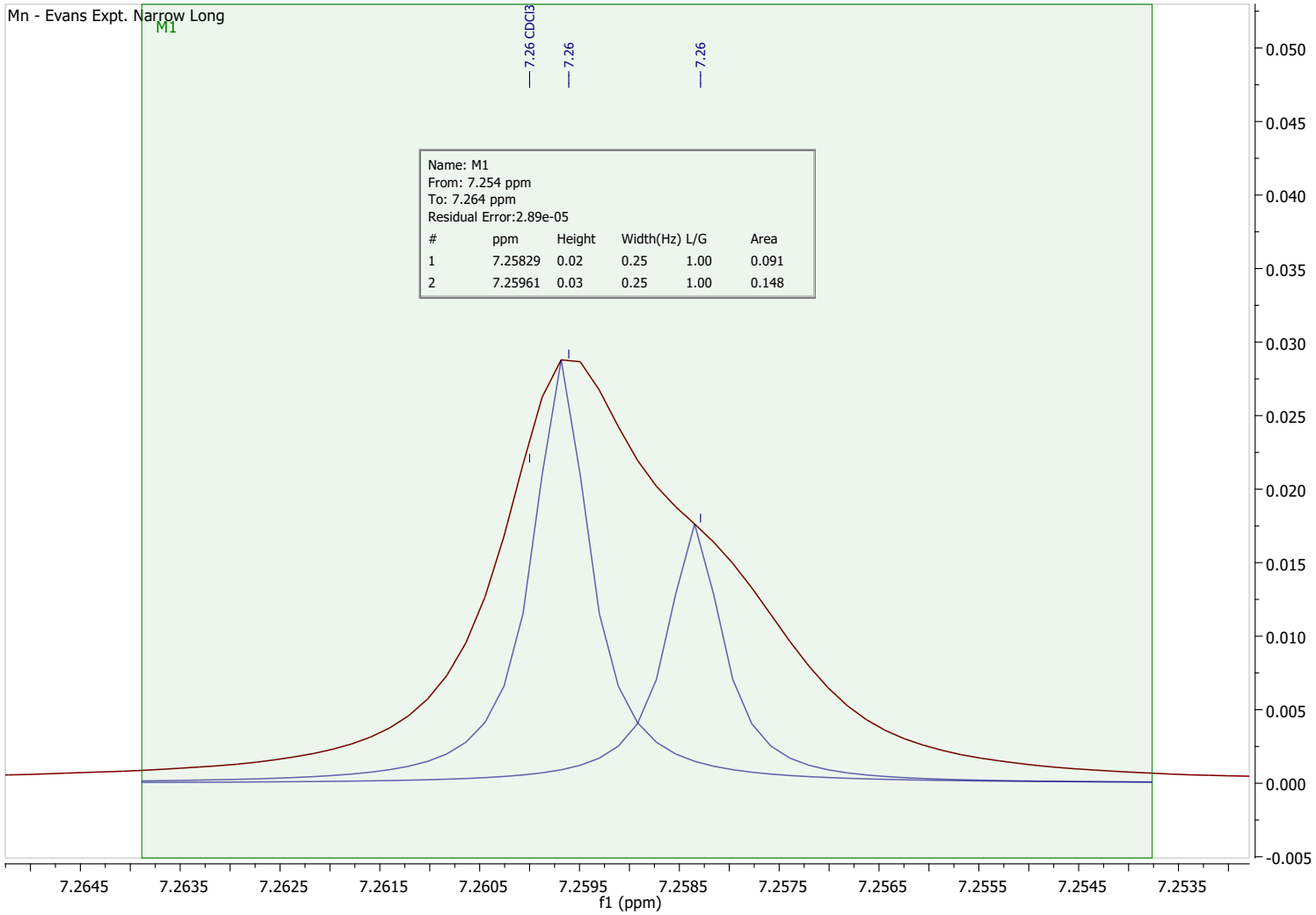

Figure S35. Expansion of ^{1}H NMR spectrum of complex **3** (Mn), along with peak fitting used for calculations. (298K, $CDCl_3$, 400 MHz).

3·3.5DMF		
Mass	0.0138	g
Formula weight	1441.18	g mol^{-1}
Number of moles	9.575E-06	mol
Vol. NMR	0.0006	L
Conc. NMR	1.596E-02	M
f1	7.25961	ppm
f1	2905295922	Hz
f2	7.25829	ppm
f2	2904767658	Hz
F	400200000	Hz
Δf	528264	Hz
χ_m	1.264E-07	
μ_{eff} *(obs.)*	4.82	μ_B
For LS Mn^{III}	2.83	μ_B
For HS Mn^{III}	4.90	μ_B
1 x HS Mn^{III} ***observed via magnetic moment***		

$$Eq.\ (1)\ \ \chi_m = \frac{6\ \ \Delta f}{1000 cF}$$

$$Eq.\ (2)\ \mu_{eff} = 798\sqrt{\chi_m T}$$

$$Eq.\ (3)\ \mu_{eff} = \sqrt{n(n+2)}$$

Δf	Difference in shift	Hz
F	Frequency of spectrometer	Hz
c	Concentration of analyte solution	M
χ_m	Molar magnetic susceptibility	$m^3\ mol^{-1}$
T	Temperature	K
μ_{eff}	Effective magnetic moment	μ_B (Bohr magnetons)
n	Number of unpaired electrons	Unitless

Table. S3. Calculations and Data for determination of magnetic susceptibility *via* the Evans NMR Method.[S12]

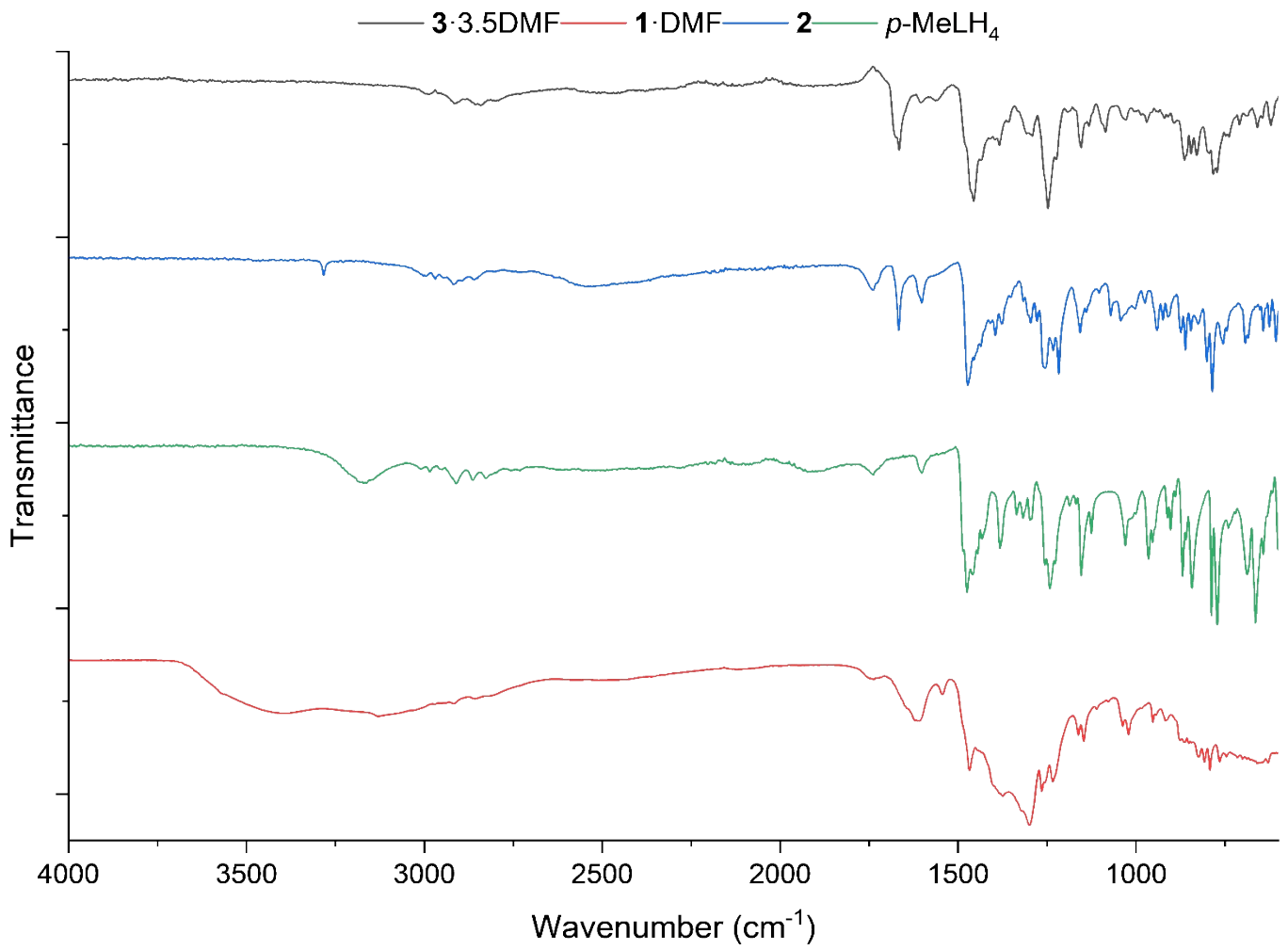

Figure S36. ATR-FT-IR Spectra of **1** - **3** and $\mathbf{L^1H_4}$ (4000–600 cm^{-1}).

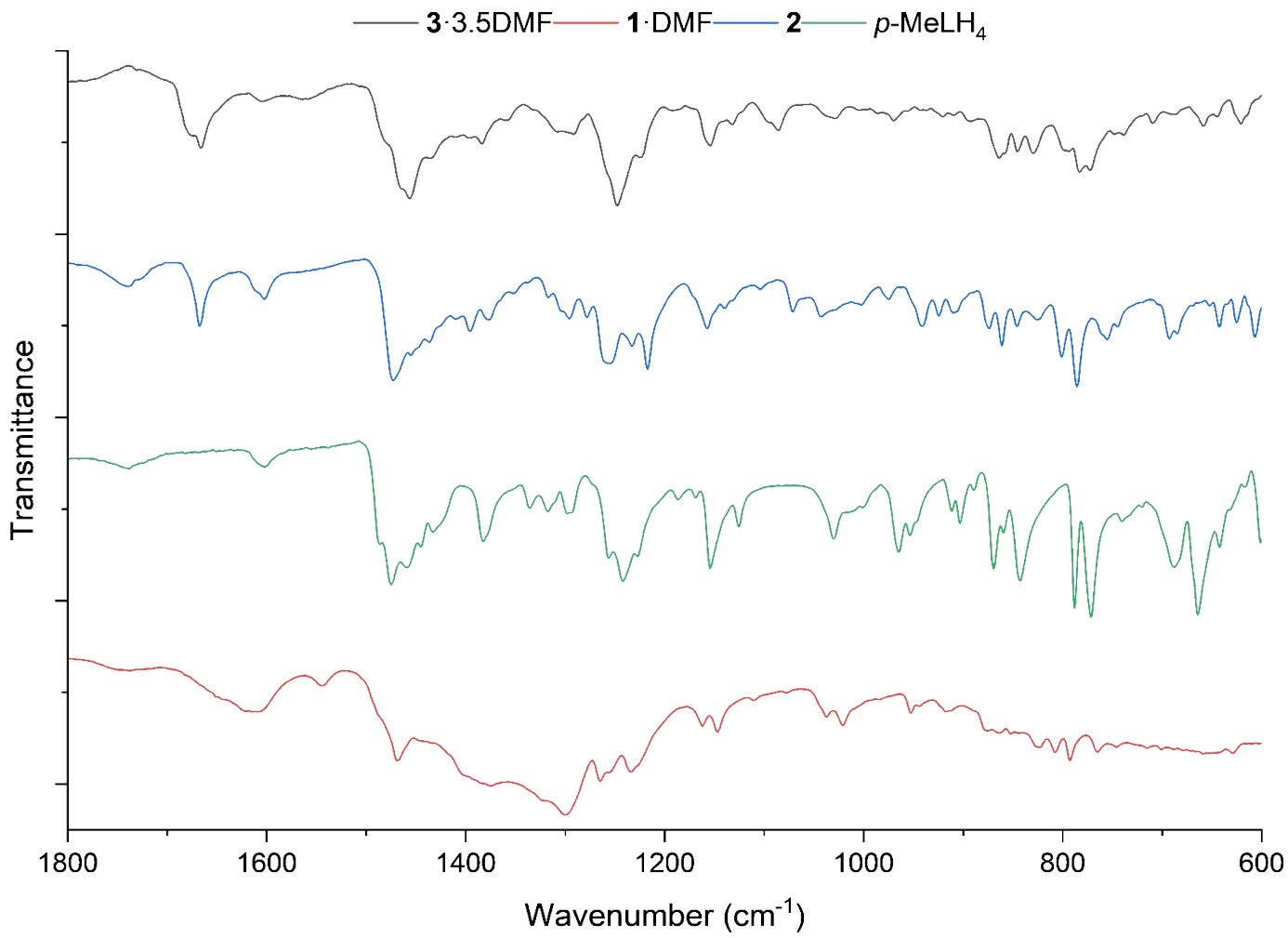

Figure S37. Expansion of the fingerprint region of the ATR-FT-IR Spectra of **1** - **3** and $\mathbf{L^1H_4}$ (1800–600 cm^{-1}).

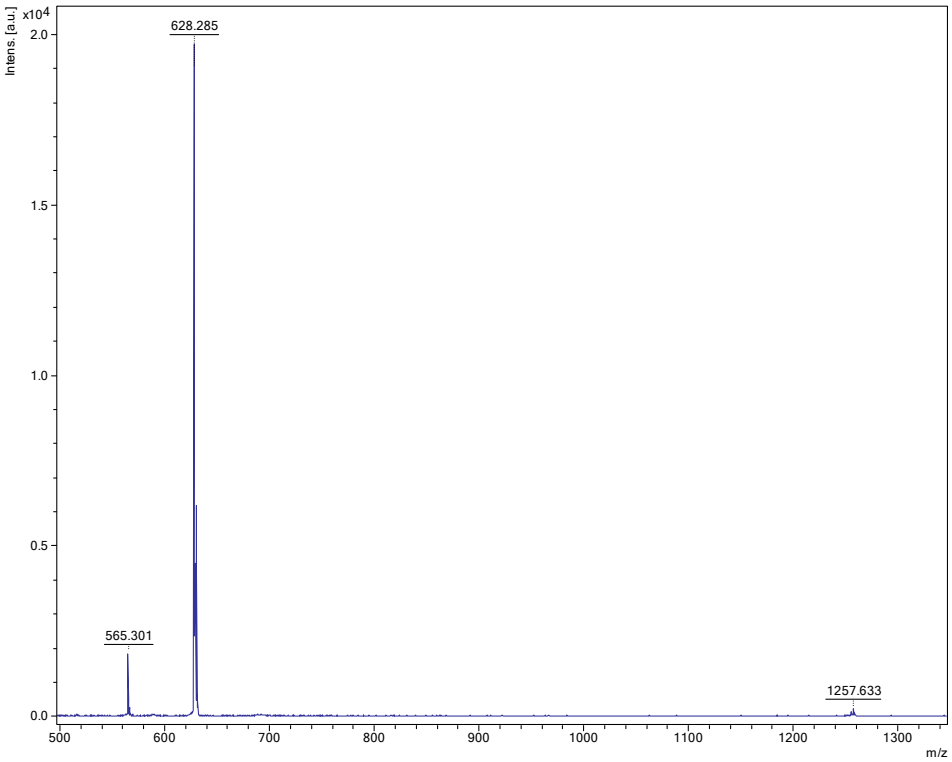

Figure S38. MS (MALDI-ToF) for **1**·DMF.

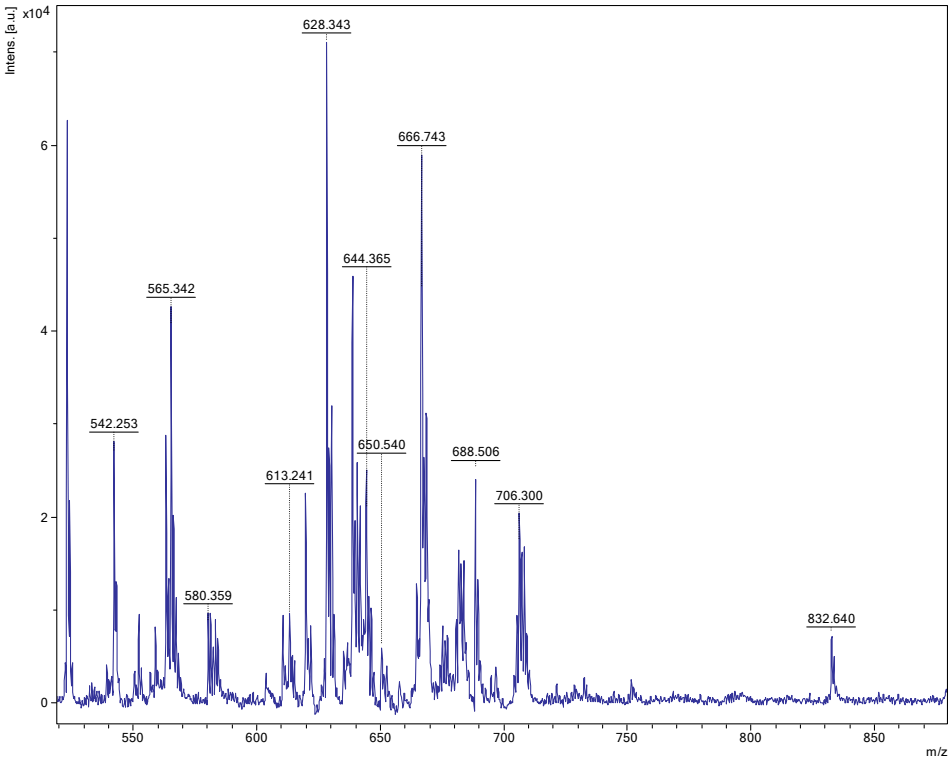

Figure S39. MS (MALDI-ToF) for **2**.

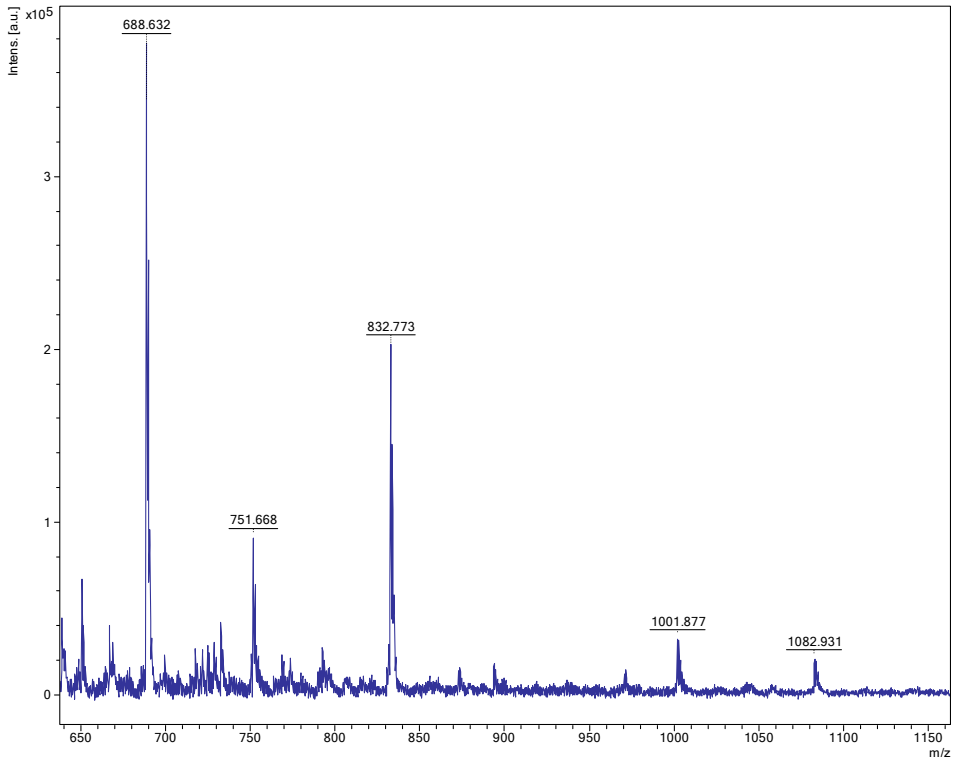

Figure S40. MS (MALDI-ToF) for **3**·3.5DMF.

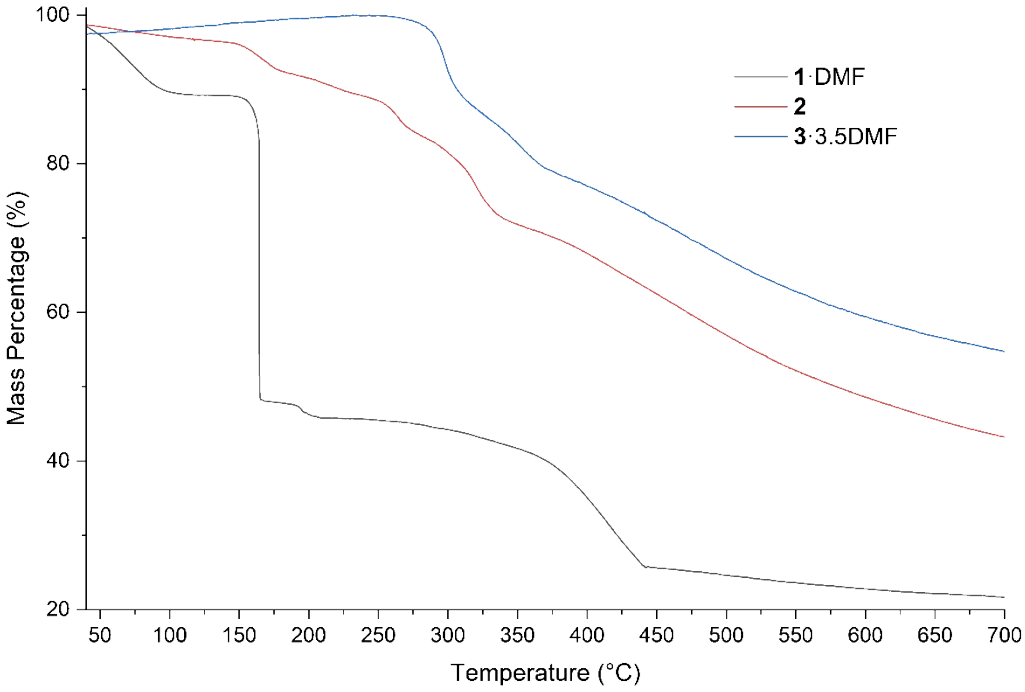

Figure S41. TGA analysis of **1**·DMF, **2**, and **3**·3.5DMF.

References

[S1] H. Takemura, A. Takahashi, H. Suga, M. Fukuda, T. Iwanaga, Synthesis of Azacalixarenes through Dihydrobenzoxazine Derivatives of Phenols, *Eur. J. Org. Chem*. 2011, **2011**, 3171–3177. DOI: org/10.1002/ejoc.201001688

[S2] G. Karotsis, S. J. Teat, W. Wernsdorfer, S. Piligkos, S. J. Dalgarno, E. K. Brechin, Calix[4]arene-Based Single-Molecule Magnets, *Angew. Chem. Int. Ed*. 2009, **48**, 8285–8288; DOI: org/10.1002/anie.200904094; *Angew. Chem*. 2009, **121**, 8435–8438.DOI: org/10.1002/ange.200904094

[S3] CrysAlisPro: CrysAlisPro 1.171.43.143a (Rigaku Oxford Diffraction, 2024)

[S4] G. M. Sheldrick, SHELXT– Integrated space-group and crystal structure determination. *Acta Cryst*. 2015, **A71**, 3-8. Doi: org/10.1107/S2053273314026370

[S5] G. M. Sheldrick, Crystal structure refinement with SHELXL: *Acta Cryst*. 2015, **C71**, 3-8. Doi: org/10.1107/S2053229614024218

[S6] O. V. Dolomanov, L. J. Bourhis, R. J., Gildea, J.A. K. Howard and H. Puschmann, Olex2. *J. Appl. Cryst*. 2009, **42**, 339-341. Doi: 10.1107/S0021889808042726

[S7] H. Takemura, T. Iwanaga, T. Shinmyozu, Structures and C–H···π interactions in DMF inclusion complexes of homoazacalix[4]arenes. *Tetrahedron Lett.*, 2005, **46**, 6687–6690. Doi: 10.1016/j.tetlet.2005.07.144

[S8] S.-L. Lee, F.-L. Hu, X.-J. Shang, Y.-X. Shi, A. L. Tan, J. Mizera, J. K. Clegg, W.-H. Zheng, D. J. Young and J.-P. Lang, Efficient ring-opening polymerization (ROP) of ε-caprolactone catalysed by isomeric pyridyl β-diketonate iron(III) complexes. *New J. Chem*. 2017, **41**, 14457-14465. Doi: 10.1039/c7nj03571c

[S9] K. Żółtowska, M. Sobczak, E. Olędzka, Novel zinc-catalytic systems for ring opening polymerization of ε-caprolactone. *Molecules* 2015, **20**, 2816-2827. Doi: 10.3390/molecules20022816

[S10] T. J. Prior and C. Redshaw, Tin complexes derived from the acids $Ph_2C(X)CO_2H$ (X = OH, NH_2): structure and ROP capability. *Catalysts* 2025, **15**, 261. Doi: org/10.3390/catal15030261

[S11] a) C.-H. Huang, F.-C. Wang, B.-T. Ko, T.-L. Yu, and C.-C. Lin. Ring-Opening Polymerization of ε-Caprolactone and *L*-Lactide Using Aluminum Thiolates as Initiator. *Macromolecules* 2001, **34**, 356–361. Doi: org/10.1021/ma0014719; (b) M. Save, M. Schappacher and A. Soum. Controlled Ring-Opening Polymerization of Lactones and

Lactides Initiated by Lanthanum isopropoxide, 1. General Aspects and Kinetics. *Macromol. Chem. Phys*. 2002, **203**, 889–899. Doi: org/10.1002/1521-3935(20020401)203:5/6<889::AID-MACP889>3.0.CO;2-O

[S12] D. F. Evans, The determination of the paramagnetic susceptibility of substance in solution by nuclear magnetic resonance. *J. Chem. Soc*. 1953, 2003-2005. DOI: org/10.1039/JR9590002003